UNITED NATIONS EDUCATIONAL, SCIENTIFIC AND CULTURAL ORGANIZATION
INTERNATIONAL ATOMIC ENERGY AGENCY
INTERNATIONAL CENTRE FOR THEORETICAL PHYSICS
I.C.T.P., P.O. BOX 586, 34100 TRIESTE, ITALY, CABLE: CENTRATOM TRIESTE

SMR/1006 - 14

COURSE ON "OCEAN-ATMOSPHERE INTERACTIONS IN THE TROPICS"
26 May - 6 June 1997

"Interannual Variability in a Tropical Atmosphere-Ocean Model: Influence of the Basic State, Ocean Geometry & Nonlinearity"

D. BATTISTI
Dept of Atmospheric Sciences
University of Washington
Seattle WA
USA

Please note: These are preliminary notes intended for internal distribution only.

Reprinted from JOURNAL OF THE ATMOSPHERIC SCIENCES, Vol. 46, No. 12, 15 June 1989
American Meteorological Society

Interannual Variability in a Tropical Atmosphere–Ocean Model: Influence of the Basic State, Ocean Geometry and Nonlinearity*

DAVID S. BATTISTI†

Dept. of Atmospheric Sciences, University of Washington, Seattle, Washington

ANTHONY C. HIRST

Joint Institute for the Study of the Atmosphere and Ocean, University of Washington, Seattle, Washington

(Manuscript received 18 May 1988, in final form 22 November 1988)

ABSTRACT

The behavior of a tropical coupled atmosphere/ocean model is analyzed for a range of different background states and ocean geometries. The model is essentially that of Cane and Zebiak for the tropical Pacific, except only temporally constant background states are considered here. For realistic background states and ocean geometry, the model solutions feature oscillations of period of 3–5 yr. By comparing the full model solution with a linearized version of the model, it is shown that the basic mechanism of the oscillation is contained within linear theory.

A simple linear analog model is derived that describes the nature of the interannual variability in the coupled tropical atmosphere–ocean system. The analog model highlights the properties that produce coupled atmosphere–ocean instability in the eastern ocean basin, and the equatorial wave dynamics in the western ocean basin that are responsible for a delayed, negative feedback into this instability growth. The growth rate of the local instability c, together with the magnitude b and lag τ of the wave-induced processes determine the nature of the interannual variability displayed in the coupled model. Specifically, these processes determine the growth rate of the *coupled* system and, when the solutions are oscillatory, the period of the oscillation. The terms b, c, and τ are set by the background state of the atmosphere and ocean, and the geometry of the ocean basin.

The simple analog model is used to design and interpret a set of experiments using the full linear and nonlinear numerical models of the coupled atmosphere–ocean system in the Pacific. In these experiments, we examine the effects of the assumed basic state and ocean geometry on the interannual variability of the coupled system. The simple model is shown to be a remarkably good proxy of the full linear and nonlinear numerical models. The limiting nonlinearity in the full numerical model is shown to be the dependence of the temperature of the upwelled water on the thermocline depth. However, we find the essential processes that describe the local instability growth rate and period of the interannual oscillations in the coupled system are linear. Nonlinearities primarily act as a bound on the amplitude of the final state oscillations, and decrease the period of the final state oscillations by about 10 percent from that obtained in the small amplitude regime of the full coupled model and the linear analog model. The nonlinear analog model for the full numerical model is derived, and compared with that proposed by Suarez and Schopf. The numerical and analog models help to explain why organized, large amplitude, interannual variability is prominent in the tropical Pacific basin, and not in Atlantic and Indian basins.

1. Introduction

In an earlier study, Battisti (1988a) identified the dynamics and thermodynamics that were acting in a coupled tropical atmosphere–ocean model that exhibited interannual variability similar to El Niño–Southern Oscillation (ENSO). In that paper, a series of numerical experiments were done to ascertain the processes that were central in producing the model interannual variability. The model used was a simple coupled ocean–atmosphere model, very similar to that of Cane and Zebiak (1985) and Zebiak and Cane (1987). In agreement with the results of Cane and Zebiak, warm events are initiated in the spring prior to the event peak, and appear well described as an instability of the coupled system. During instability growth, a positive sea surface temperature (SST) anomaly in the equatorial eastern Pacific produces westerly wind anomalies in the equatorial central Pacific which in turn generates a downwelling Kelvin wave that suppresses the pycnocline to the east. SST is very sensitive

* Contribution No. 43 to the Joint Institute for the Study of the Atmosphere and Ocean.

† Current affiliation: Joint Institute for the Study of the Atmosphere and Ocean, AK-40, University of Washington, Seattle, WA 98195.

Corresponding author address: Dr. David Battisti, Department of Meteorology, University of Wisconsin, 1225 W. Dayton St, Madison, WI 53706.

to pycnocline depth in the eastern model Pacific; a deeper pycnocline induces warmer surface water via modulation of vertical temperature advection. Thus the suppression of the pycnocline resulting from the westerly wind anomalies leads to still larger SST anomalies.

In this numerical model, oceanic wave dynamics determines the fate of the growing coupled instability. The aforementioned westerly wind anomalies also produce equatorially trapped Rossby waves that propagate freely to the western boundary. These waves reflect at the western boundary, sending upwelling equatorial Kelvin waves back to the central basin. These cooling Kelvin waves act to terminate instability growth and rapidly plunge the coupled system into a cold regime. The western boundary reflection is necessary for event termination. The system returns from a cold regime via reduced heat flux to the atmosphere and, to a lesser extent, by wave-induced processes like that which lead to the warm event termination.

The aforementioned dynamical description of ENSO evolution is not unique to the Cane and Zebiak model. Schopf and Suarez (1988) used a more complicated numerical model of the coupled tropical atmosphere–ocean system than Battisti. They described a dynamical scenario for ENSO events occurring in their model that is very similar to that Battisti described occurring in the Cane and Zebiak (1985) model. Additionally, there is preliminary evidence that this dynamical scenario is relevant to *some* ENSO events observed in coupled general circulation models of the atmosphere and ocean (S. G. H. Philander 1988, personal communication).

With the studies of Zebiak and Cane (1987), Schopf and Suarez (1988) and Battisti (1988a) in mind, we will explore in this paper how the local instability operating in the eastern basin interacts with the signal reflected from the western boundary to set the period and growth rate displayed by the coupled system. This is done, in part, by deriving a set of simple analog models for the coupled tropical atmosphere–ocean system from the full numerical model of Battisti (1988a, hereafter B88), due to Zebiak and Cane (1987). We will find that the essential physics in the coupled model is described by a linear delayed oscillator equation, in contrast to the fundamentally nonlinear delay oscillator equation proposed for ENSO by Schopf (1987) and Suarez and Schopf (1988). We will use both the linear analog model and the full numerical coupled atmosphere–ocean model to examine the behavior of the coupled tropical atmosphere–ocean system by considering various background states for the atmosphere or ocean. We will examine the sensitivity of the interannual variability in the coupled model to the efficiency of the oceanic wave reflection at the western oceanic boundary and examine how the nature of the interannual variability depends on the size of the oceanic basin. We will identify the important nonlinearity in the full numerical model, and derive the leading order nonlinear analog model for ENSO appropriate for the full coupled numerical model–a nonlinear delayed oscillator equation. The nonlinear analog model, while similar in form to that heuristically developed for ENSO by Schopf (1987) and Suarez and Schopf (1988), will highlight a very different balance in the fundamental processes than in the latter studies. We will use the nonlinear analog model to examine the secondary role of nonlinearity in the ENSO cycle in the full numerical model.

The outline of the paper is as follows. In section 2, we derive a simple linear analog model that describes the behavior of the coupled atmosphere–ocean system in various "basic states," and use this model as a guideline to design and interpret a set of experiments in which we will explore the effects of the basic state of the atmosphere and ocean on the resultant interannual variability. These experiments are presented in section 3. Several nonlinear oscillator models for ENSO events in the full model is derived in section 4, and compared to that postulated by Schopf (1987) and Schopf and Suarez (1988). The conclusions and a discussion are found in section 5.

2. A simple analog model of the coupled atmosphere–ocean system

In this section we present a simple stability analysis of the coupled system that enables a qualitative description of the behavior of the coupled system with different basic states. We will include the essential thermodynamics and dynamics of the system, identified in B88, to derive a single, first-order differential equation for the behavior of the coupled system in terms of the sea surface temperature anomaly (SST) in the eastern equatorial Pacific.

a. The linear analog model

We begin by reviewing the geometry of the system. To lowest order, the sea surface temperature (SST), zonal wind stress τ^x, and pycnocline perturbation h anomalies change uniformly throughout the eastern basin in the equatorial band. SST and τ^x display an in-phase relationship with one another, whereas h tends to lead SST and τ^x slightly. In addition, we note that west of the dateline there is very little signal in the model SST or in the wind stress anomaly. Analysis of the ocean modes indicated free wave propagation west of the dateline. Finally, we will make use of the fact that the essential ocean physics and thermodynamics is contained within the equatorial band (within 5° of the equator) and that the atmospheric winds outside of the equatorial band do not affect the overall character of the interannual variability in the coupled system (see experiment 10, B88).

To further simplify the problem, we will consider a basic state in the atmosphere and ocean that is constant in time; the seasonal cycle is replaced with a simple

annual average. Recall that the seasonal cycle primarily acts to quantize the period of the interannual variability, but is not essential to producing the interannual variability. With a time-mean basic state, the model displays perfectly periodic behavior (experiment 3 of B88). We also linearize the ocean thermodynamics and coupling between the two media. A comparison of solutions from linear and nonlinear versions of the full model, presented in section 3, will demonstrate that the basic mechanism of oscillation is contained within linear theory.

The aforementioned characteristics of the coupled system led us to consider the following simple system. The ocean is approximated as two boxes centered on the equator. One box represents the "western Pacific," spanning from 160°W to ~125°E, where waves are assumed to propagate freely. In this box, there are no SST or overlaying wind stress anomalies. In the eastern box, spanning 160°W to ~80°W, SST and pycnocline anomalies occur. The SST anomalies drive a zonal wind stress anomaly, τ^x, that acts throughout the eastern patch of the ocean. Finally, since the pertinent dynamics and thermodynamics happen in a thin equatorial band, and rather homogeneously throughout the eastern box, we further reduce the problem by considering the area averaged quantities $\langle T\rangle$ and $\langle \tau^x\rangle$, where $\langle * \rangle$ denotes an area averaging.

The linearized equation for the model SST is

$$\frac{\partial T}{\partial t} = -\bar{\mathbf{u}}\cdot\nabla T - \mathbf{u}\cdot\nabla\bar{T} - \delta\Delta(\bar{w})\frac{\partial T}{\partial z} - \delta H(\bar{w})w\frac{\partial\bar{T}}{\partial z} - \alpha_s T, \quad (2.1)$$

where

$$\Delta(x) = \begin{cases} x, & x > 0 \\ 0, & x \leqslant 0, \end{cases} \qquad H(x) = \begin{cases} 1, & x > 0 \\ 0, & x \leqslant 0 \end{cases}$$

and T is the SST anomaly, $\mathbf{u}$ the horizontal current, w the upwelling velocity, α_s a measure of the thermal damping rate, and t is time; ∇ is the horizontal operator $\mathbf{i}\partial/\partial x + \mathbf{j}\partial/\partial y$ where x and y are positive east and north respectively, z is the vertical coordinate, and δ a mixing efficiency coefficient ($\delta = 0.75$). Overbars denote time-mean basic state quantities. (Discussion of the full nonlinear model SST equation are found in B88 and Zebiak and Cane 1987.) The terms on the right hand side of (2.1) are, from left to right, advection of the anomalous horizontal temperature gradient by the mean currents, advection of the mean horizontal temperature gradient by the anomalous currents, mean upwelling acting on the anomalous vertical temperature gradient, anomalous upwelling on the mean vertical temperature gradient, and thermal damping. The linearized anomalous vertical temperature gradient is given by

$$\frac{\partial T}{\partial z} = \frac{T - T_s}{H_1} = \frac{T - a(\bar{h})h}{H_1},$$

where T_s is an anomalous subsurface temperature that results from movement of the subsurface pycnocline and H_1 is the thickness of the ocean mixed layer [T_s is defined in (4.2), and linearized to $a(\bar{h})h$ in appendix C]. Constant upwelling, $\bar{w}$, on a weaker $\partial(\bar{T}+T)/\partial z$ will produce less cooling than in the mean, and therefore produce anomalous warming. In this model, the upper layer thickness anomaly h acts as a proxy for the pycnocline perturbations, and can be written in linearized form as $T_s = a(\bar{h})h$ [see Eq. (4.2)]. Hence the linearized equation for the SST anomaly in the eastern box is

$$\frac{\partial T}{\partial t} = -\bar{u}\frac{\partial T}{\partial x} - \frac{\partial\bar{T}}{\partial x}u - \bar{v}\frac{\partial T}{\partial y} - \delta\frac{\Delta(\bar{w})}{H_1}T + \frac{\delta\Delta(\bar{w})a(\bar{h})}{H_1}h - \delta H(\bar{w})\frac{\partial\bar{T}}{\partial z}w - \alpha_s T. \quad (2.2)$$

The very small term $(\partial\bar{T}/\partial y)v$ has been dropped from (2.2) (see B88, section 2c).

We now consider the evolution of the SST averaged over the eastern equatorial Pacific box:

$$\frac{\partial\langle T\rangle}{\partial t} = -\pi_1\frac{\langle\bar{u}\rangle}{L_x}\langle T\rangle - \pi_2\left\langle\frac{\partial\bar{T}}{\partial x}\right\rangle\langle u\rangle - \pi_3\frac{\langle\bar{v}\rangle}{L_y}\langle T\rangle - \delta\pi_4\frac{\langle\Delta(\bar{w})\rangle}{H_1}\langle T\rangle + \frac{\delta\pi_5}{H_1}\langle\Delta(\bar{w})a(\bar{h})\rangle h - \pi_6\delta\left\langle H(\bar{w})\frac{\partial\bar{T}}{\partial z}\right\rangle\langle w\rangle - \alpha_s\langle T\rangle. \quad (2.3)$$

Since, in general, all the field variables in (2.2) have a rich horizontal structure, the spatial correlation between various quantities must be taken into account when writing (2.3) in terms of the time dependent variables and the time mean coefficients. This gives rise to the π_i coefficients that are defined, for example, as

$$\pi_4 = \frac{\langle\Delta(\bar{w})T\rangle}{\langle\Delta(\bar{w})\rangle\langle T\rangle}.$$

These coefficients are somewhat sensitive to the size of the box in which we spatially average. The sensitivity of our results to the box size is addressed later on. The term containing $\Delta(\bar{w})a(\bar{h})h/H_1$ in (2.3) is relatively

well defined regardless of the latitudinal extent of the box because $\Delta(\bar{w})a(\bar{h})$ is sharply peaked on the equator. Therefore, h in (2.3) is evaluated on the equator ($y = 0$), and averaged over the latitudinal extent of the box.

The upper-layer depth changes in the model result directly from wind stress anomalies. In the eastern Pacific, changes in h can be considered due to local processes (these include wave reflection on the eastern boundary) and Kelvin waves propagating into the eastern basin from the western Pacific. These Kelvin waves result from Rossby waves that are generated in the central/eastern basin by wind stress anomalies. The Rossby waves propagate westward and are reflected at the western ocean boundary. There is little generation of waves in the western basin (see B88). Hence we can write h on the equator in terms of the local contribution, h_L, and the remote contribution, $h_{\text{reflected Kelvin}}$:

$$h = h_{\text{reflected Kelvin}} + h_L$$
$$h_{\text{reflected Kelvin}} = -a_W\langle\tau^x(t-\tau)\rangle, \quad h_L = a_L\langle\tau^x\rangle. \tag{2.4}$$

The coefficients a_W and a_L are well defined for low frequency motion and depend primarily on the longitudinal extent of the box and the assumed values of reduced gravity in the ocean. The value of a_L is found by assuming that, for low frequency motions, there is a local balance between the zonal wind stress and pressure gradient. a_W is specified using equatorial, longwave dynamics and knowledge of the reflective properties of low frequency Rossby waves on the western ocean boundary (e.g., see appendix B of B88). Later, we will come back and address the question of the effects of western boundaries that are inefficient reflectors on the interannual variability of the coupled system.

An important aspect of (2.4) is that the zonal wind stress anomaly $\langle\tau^x\rangle$ in the eastern box gives rise to a quick local change h_L in the pycnocline depth, and produces a delayed signal in h that has the opposite sign of the local response (a_L and a_W are positive), but lags the local response by τ: the time it takes for the gravest mode symmetric Rossby wave to travel from the forcing region in the central/western basin to the western boundary and the reflected Kelvin wave to return from the boundary to the eastern basin. We will refer to τ as the wave transit time, or the transit time.

There are four unknowns in (2.3): $\langle T\rangle$, h, $\langle u\rangle$ and $\langle w\rangle$. The latter three quantities are primarily functions of the zonal wind stress anomaly. To a high degree of accuracy h, $\langle u\rangle$ and $\langle w\rangle$ can be approximated as functions of the zonal wind stress anomaly which, in turn, is directly related to the SST. We make the following assumptions:

$$\langle\tau^x\rangle = \beta\langle T\rangle \tag{2.5}$$
$$w = -\gamma\langle\tau^x\rangle \tag{2.6}$$
$$\langle u\rangle = \frac{r_S}{\rho_0 H_1}\left\langle\frac{\tau^x}{r_S^2+f^2}\right\rangle \approx \frac{\langle\tau^x\rangle}{\rho_0 H_1 r_S}. \tag{2.7}$$

In (2.7), f is the Coriolis parameter, ρ_0 the density of water and r_S^{-1} a linear damping time (see Zebiak and Cane 1987). The relation (2.7) produces a qualitative representation of the surface current field in the equatorial Pacific band on monthly time scales. The relations (2.5) and (2.6) are extremely accurate for the fields $\langle w\rangle$, $\langle\tau^x\rangle$ and $\langle T\rangle$ (Fig. 1). Inserting the ex-

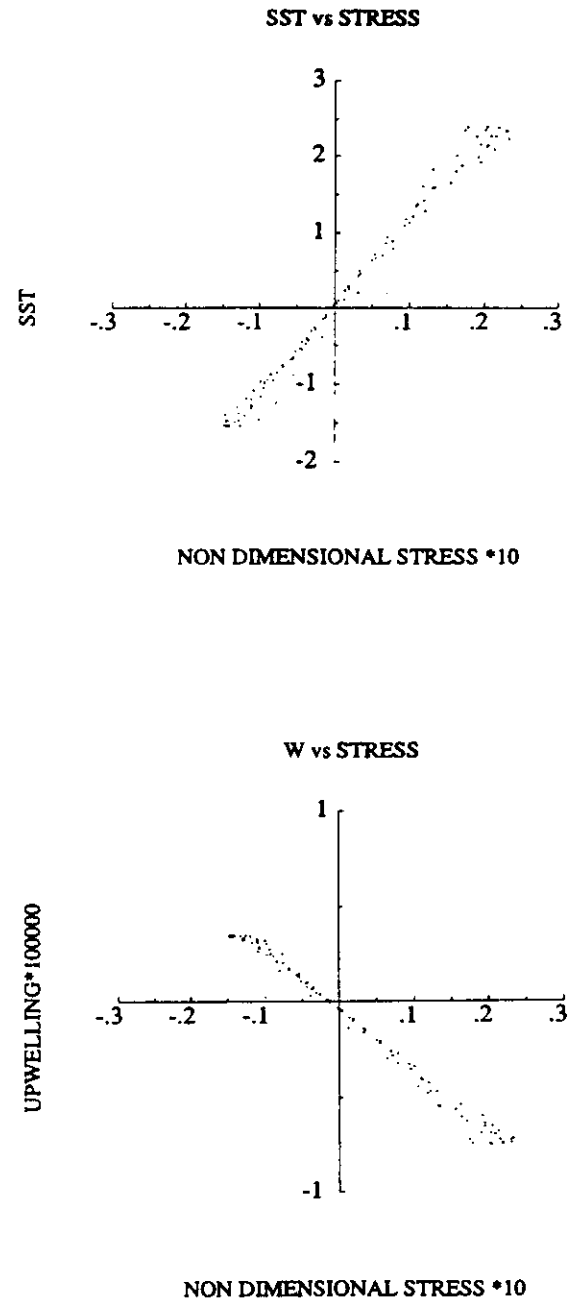

FIG. 1. (a) A plot of sea surface temperature $\langle T\rangle$ vs nondimensional zonal wind stress $\langle\tau^x\rangle$, averaged over the equatorial box, 2°N to 2°S, 80° to 180°W. The data is from the full nonlinear coupled model solutions with a time-mean (seasonless) basic state. A nondimensional wind stress of 0.1 corresponds to a wind stress anomaly of 0.1 dynes cm^{-2}. (b) As in panel (a), but for anomalous upwelling rate $\langle w'\rangle$ vs $\langle\tau^x\rangle$. Units of upwelling are m s^{-1}.

presssions (2.4), (2.5), (2.6), (2.7) into (2.3), a single ordinary differential equation for $\langle T \rangle$ is obtained (the $\langle * \rangle$ notation is dropped):

$$\frac{\partial T}{\partial t} = -\hat{K}T + K(-a_W \beta T(t-\tau) + a_L \beta T) + K_E \gamma \beta T + K_A T - \alpha_s T, \quad (2.8)$$

where

$$K \equiv \frac{\delta \pi_5}{AH_1} \int_A \int \Delta(\bar{w}) a(\bar{h}) dA$$

$$K_E \equiv \frac{\delta \pi_6}{A} \int_A \int H(\bar{w}) \frac{\partial \bar{T}}{\partial z} dA$$

$$\hat{K} = \frac{\delta \pi_4}{AH_1} \int_A \int \Delta(\bar{w}) dA$$

$$K_A = -\frac{\beta r_S \pi_2}{A \rho_0 H_1} \int\int_A \frac{\partial \bar{T}}{\partial x} \frac{1}{r_S^2 + f^2} dA - \frac{\pi_3}{AL_y} \int_A \int \bar{v}\, dA - \frac{\pi_1}{AL_x} \int_A \int \bar{u} dA.$$

The values of the coefficients K, $\hat{K}$, K_E, K_A, σ_s, τ, a_W and a_L are set by the basic state of the model ocean and atmosphere, and the size of the oceanic basin. The coefficients γ and β are calculated from the full model runs, and are surprisingly insensitive to the area over which we average. Values for these parameters are listed in Table 1 for an eastern Pacific box that extends from 180°W to the eastern coastline, 2° about the equator. The range of values cited in the table result from considering various ocean boxes for averaging.

Equation (2.8) is written more compactly as

$$\boxed{\frac{\partial T}{\partial t} = -bT(t-\tau) + cT}, \quad (2.9)$$

TABLE 1. Values for the model coefficients used in the evaluating the terms b and c in Eq. (2.9). The basic state coefficients are derived from the time-mean equatorial Pacific ocean currents upwelling and surface wind field. The regression coefficients are derived from the full numerical atmosphere/ocean model described in section 2.

Coefficient	Value	Range
	Basic state coefficients	
K	2.7×10^{-8} °C m^{-1} s^{-1}	1.5 to 3.0 $\times 10^{-8}$
K_E	2.5×10^{-2} °C m^{-1}	2.2 to 2.8 $\times 10^{-2}$
$\hat{K}$	1.8×10^{-7} s^{-1}	1.4 to 2.2 $\times 10^{-7}$
K_A	7.3×10^{-8} s^{-1}	4.0 to 8.0 $\times 10^{-8}$
a_W	490 m^3 N^{-1}	440–540
a_L	750 m^3 N^{-1}	700–800
a_s	9.1×10^{-8} s^{-1}	
τ	180 days	
	Regression values	
γ	3.3×10^{-4} m^3 N^{-1} s^{-1}	3.0 to 3.6 $\times 10^{-4}$
β	9.5×10^{-3} N m^{-2} °C^{-1}	9. to 10. $\times 10^{-3}$

where

$$b = \underset{[3.9]}{a_W \beta K} \qquad c = \underset{[6.0]}{\beta a_L K} + \underset{[2.5]}{\beta \gamma K_E} + \underset{[2.3]}{K_A} - \underset{[5.7]}{\hat{K}} - \underset{[2.9]}{\alpha_s}.$$

The numbers below each term in the definition of b and c denote the value of each term for the basic state of the Pacific atmosphere–ocean (units are yr^{-1}). Assuming a solution of the form $T = T_0 e^{\sigma t}$ we obtain the following equation

$$\sigma = -be^{-\sigma\tau} + c. \quad (2.10)$$

Equation (2.9) describes a delayed oscillator: the characteristics of the solution depend critically on the values of b and c. For our system, the term b describes the effects of the Kelvin waves propagating into the eastern box from the western box. The importance of the wave-induced effects depends on the amplitude of the incoming waves and the lag between wave generation and arrival in the eastern basin (via reflection off the western boundary). The term c is the sum of all the processes that induce local changes in the SST in the eastern box (all variables are positive), and represent the following processes:

$\beta a_L K - \hat{K}$	mean upwelling on an anomalous vertical temperature gradient (local wave effects are included)
$\beta \gamma K_E$	anomalous upwelling on the mean vertical temperature gradient
K_A	horizontal advection
α_s	thermal damping

In evaluating the coefficients b and c, it is worthwhile to note that the relative size of each of the individual terms that affect local instability growth is consistent with the analysis of the full model ocean thermodynamics in B88: the upwelling terms (K and K_E) are large compared to the horizontal advection terms (K_A).

b. *Properties of the delayed oscillator*

Equation (2.10) describes, in general, an oscillatory system experiencing exponential growth or decay. In the absence of remote processes ($b = 0$), (2.10) describes a pure exponential growth or decay rate c. If $c > 0$, the sum effects of upwelling and horizontal advection dominate the thermal damping and growth will occur. If $c < 0$, the thermal damping overwhelms the growth terms, and exponential decay results.

To consider the behavior of the system when the growth rates are small, we multiply (2.10) by its complex conjugate and, writing $\sigma = \sigma_r + i\sigma_i$, ($\sigma_r$, σ_i real), obtain:

$$(\sigma_r - c)^2 + (\sigma_i)^2 = b^2 e^{-2\tau\sigma_r}.$$

We see that for small growth rates, $\sigma_r \ll |c|$, in a basic state dominated by local instability processes, $b \ll |c|$,

no oscillatory solutions are possible. On the other hand, for small growth rates ($\sigma_r \ll 1$) in a basic state where local instability processes sum to be small compared to the changes induced by the remote Kelvin waves ($b \gg |c|$) oscillatory motion is possible, the period of which is

$$\frac{2\pi}{\sigma_i} = \frac{2\pi}{(b^2 - c^2)^{1/2}}.$$

Hence even if local instability processes do not favor growth ($c < 0$), oscillatory, slow growth solutions can be found for $c > -be^{-\sigma_r \tau}$ because of the "remote" wave processes b. For the parameter range of interest, the relevant oscillatory, growing solution to (2.10) is displayed in Fig. 2 for various values of b and c. A more complete discussion of the properties of (2.9) is presented in appendix A.

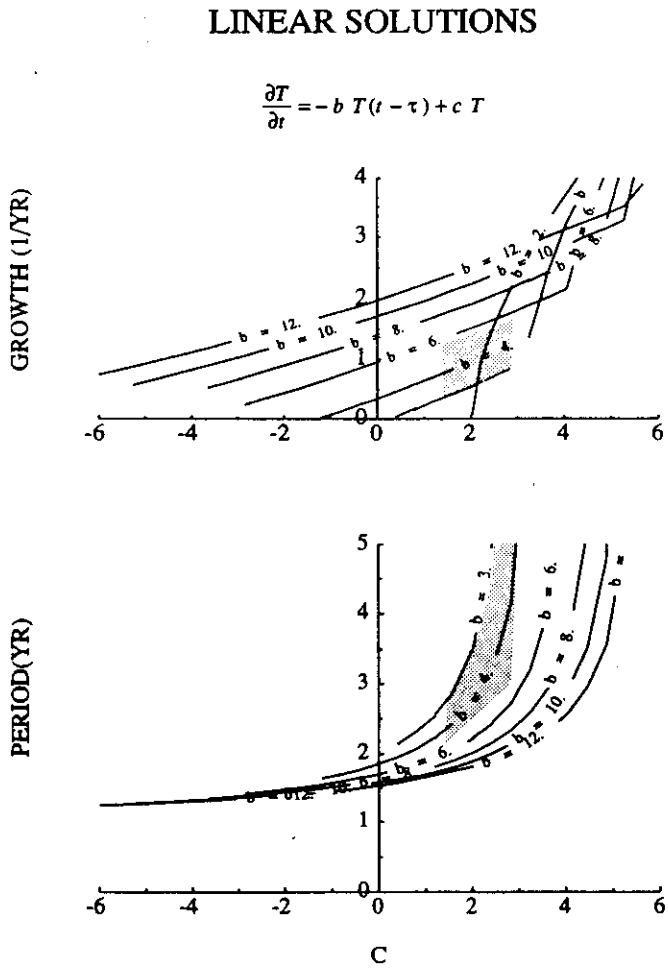

FIG. 2. The complex solutions to the delayed oscillator equation (2.10) with a reference value of τ = 180 days. The growth rate of the system (in yr^{-1}) vs the strength of the local instability term c (in yr^{-1}) is plotted in (a), and the period of the oscillation (in yr) as a function of c is plotted in (b). Each curve represents a different value for b (in yr^{-1}). For $b \approx 1.8$ yr^{-1}, solutions are pure growth. The shading indicates the range of values for the coefficients b and c for the atmosphere–ocean system in the equatorial Pacific.

c. *Behavior of the analog model near the basic state parameter values*

For the assumed basic state of the ocean and the atmosphere, the best estimate for the variables b and c is $b = 3.9$ yr^{-1}, $c = 2.2$ yr^{-1}. Assuming the oceanic wave speed of 2.9 m s^{-1}, τ = 180 days. These estimates for b, c, and τ set the growth rate and period of oscillation to be $\sigma_r^{-1} = 1.1$ yr and $2\pi/\sigma_i = 3.0$ yr, respectively. Near these reference values for b and c, however, σ varies rapidly. The range of σ for realistic b and c is indicated by the shading in Fig. 2. We see that growth rates may range from weak growth, with period 3 to 5 yr, to growth rates of up to 1.3 yr^{-1}, and period of 2.2 to 3.2 yr, depending on the size of the box in which the averaging is done. For a realistic range of values for c, the period of oscillation may vary from 2.5 to 4.0 yr, and the growth rate from 0.6 to 1.0 yr^{-1}. Note that (2.4) states that, when there are oscillatory solutions for the coupled system, there is a phase lag between h and $\langle T \rangle$. This lag is given by expression

$$\tan^{-1}\left[\frac{a_L + a_W}{a_L - a_W}\tan\left(\frac{\sigma_i \tau}{2}\right)\right] - \frac{\sigma_i \tau}{2}.$$

For our reference state ($b = 3.9$ yr^{-1}, $c = 2.2$ yr^{-1}, τ = 180 days) in the simple model, h leads $\langle T \rangle$ by 65 days, in qualitative agreement with the full model results (about 70 days).

We shall now examine the qualitative behavior of the analog model near these reference values. For constant lag τ and magnitude of remote wave processes b, processes that increase the local instability strength c will increase the growth rate of the coupled system and decrease the period of the resultant oscillations. However, if the basic state is modified so c is greater than about 3.2 yr^{-1}, no oscillations would be possible: the system would display enhanced exponential growth from that of the reference state. For basic states with c less than -1.2 yr^{-1}, there are no solutions that display growth. Note that for our basic state, c is the small net difference between some rather large terms. This is consistent with the full model calculations of B88, where the nature of the interannual variability in the coupled system was sensitive to the horizontal advective processes, even though these processes are small compared to the vertical upwelling and thermal damping processes.

Now we hold the local instability terms constant (c = 2.2 yr^{-1}), and consider a coupled system in which the amplitude of the incoming Kelvin waves is different from that of our reference state. The simple model indicates that by decreasing the amplitude of the Kelvin waves incoming from the western boundary, the period of the oscillations will be longer than for the reference state, and the growth rate of the coupled instability will decrease. Similarly, increasing the remote wave effects acts to increase the growth rate of the system and decrease the period of oscillation.

Finally, we wish to consider the effects of the transit time τ on a basic state ocean and atmosphere with the same magnitude of local instability strength and remote wave amplitude. In this manner, we can consider the effects of the ocean basin size on the behavior of the coupled system. [Here we are actually changing the width of the western box. All the action in wind stress and SST is still occurring in the fixed width eastern box.] In Fig. 3, the growth rate and period of the coupled system are plotted as a function of the time lag τ for $b = 3.9\ \text{yr}^{-1}$. Each curve represents a different value of basic state c. For lags greater than $\tau \equiv \tau_R = 180$ days, the simple model indicates that both the growth rate and the period of oscillation should increase, while for lags smaller than τ_R, the growth rate and period should both decrease. For basic states that have much stronger net local instability growth rates ($c \gg 2.2\ \text{yr}^{-1}$), increasing τ has little effect on the growth rate of the coupled system, but changes the period markedly. We note for a wide range of values for c there is a minimum value of τ that instability growth for the coupled system is possible. For our reference state, this is about 120 days. Assuming a gravest mode ocean speed of 2.9 m s^{-1} and realistic values for b, this implies ocean basins that are smaller than about 13 000 km will not be able to host coupled ocean–atmosphere interanual variability of the kind found in our coupled numerical model.

3. Studies of the full coupled atmosphere–ocean model with various "basic states"

In this section we use the results of section 2 as a guideline to anticipate the behavior of the interannual variability in a coupled tropical atmosphere–ocean model. The coupled model we will use follows closely that described by Cane and Zebiak (1985) and Zebiak and Cane (1987), and is briefly described below. The ocean component of the model we will use consists of an upper layer, topped by a fixed depth surface (mixed) layer, overlaying a deep motionless layer. SST is calculated separately and does not directly affect the ocean dynamics. The surface currents are driven by the wind stress and retarded by Rayleigh friction. SST is changed by (nonlinear) advection by surface currents, upwelling and heat fluxes to the atmosphere. The upwelling is prescribed in terms of the divergence of the mixed layer currents and represents the entrainment into the surface layer. The upper layer, which includes the surface layer, is governed by linear shallow water wave dynamics. The atmospheric component of the model is the simple linear reduced gravity Gill (1980) model of a thermally forced tropical atmosphere. The forcing of the atmosphere depends on the total atmospheric convergence and the initial SST perturbation and is calculated iteratively (Zebiak 1986). There is no explicit time dependence in the equations that define the atmospheric variables; the atmosphere is treated as being

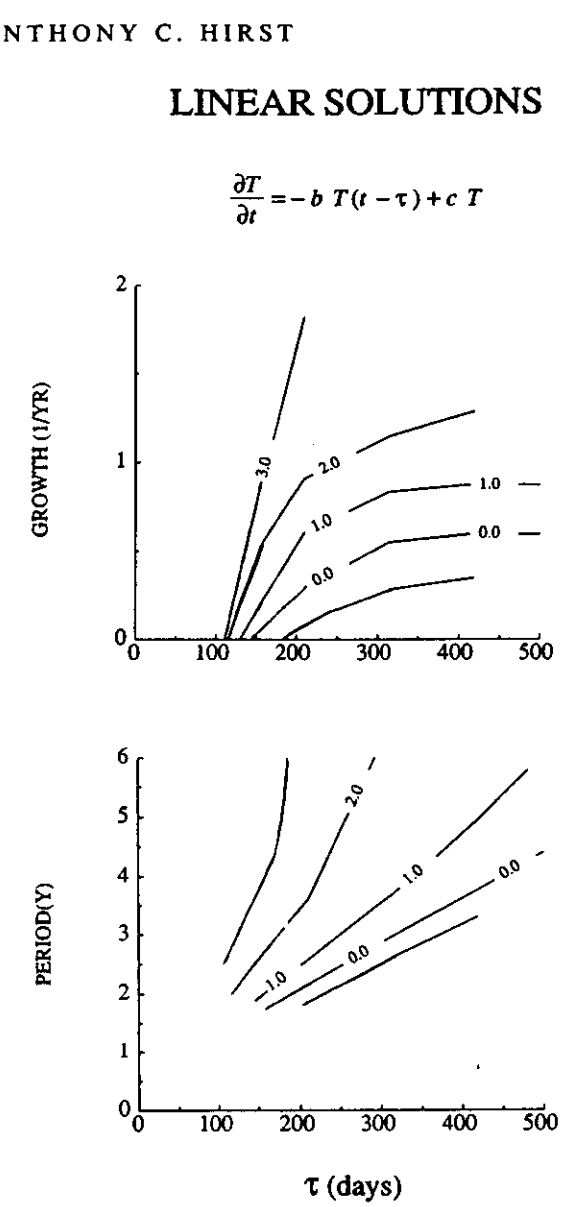

FIG. 3. The growth rate (yr^{-1}) (a) and period (yr) (b) of the coupled system vs time lag τ, for $b = 3.9\ \text{yr}^{-1}$ at $\tau = 180$ days. Each curve is for a difference reference value for c (in yr^{-1}) (for the Pacific $c = 2.2\ \text{yr}^{-1}$).

in steady state on the time scale of the ocean changes. The ocean is forced by the anomalous wind stress and the atmosphere is forced by latent heat release, which is a function of the convergence of the wind field and the SST anomaly. Both of the forcing terms are nonlinear. The ocean model domain is a rectangular basin (30°N to 30°S, 124°E to 80°W); the atmosphere is modeled on an equatorial β-plane. For a complete model description, see Zebiak and Cane (1987) or B88.

The coupled model is an anomaly model. The reference state, used to calculate the coefficients of section 2, is the time-mean (seasonless) annual current, upwelling, SST and surface wind field for the equatorial Pacific. Since we are principally interested in the growth rate and period of the variability in the coupled system, and since the simple analog model is linear, we have developed a linearized version of the nonlinear coupled

model, and will compare the behavior of the simple analog with that for both the linearized and nonlinear versions of the full coupled model. Details of the linearization are given in appendix B. Both the full linear and nonlinear models are initialized with small perturbations and then left to run free from any external forcing. The character of the solutions are independent of the form of the prescribed initial perturbation. We note that the full linear model solution is very similar to that of the full nonlinear model, except that the amplitude of the oscillation grows exponentially, without bound (Fig. 4). The full nonlinear model presently equilibrates (Fig. 5). When overall exponential growth is removed from the linear model results, the evolution of equatorial fields for the full linear model closely resembles that for the equilibrated nonlinear model (Figs. 6–8). In particular, large SST anomalies (Fig. 6) are restricted to the eastern basin, and largest windstress anomalies (Fig. 8) occur around 140°–150°W. The SST and windstress anomalies appear to develop and decay essentially in situ. Both models give a period of about 3.5 yr. The horizontal structure of the linear and nonlinear solutions are also very similar (Fig. 9). The similarity of behavior indicates the oscillation mechanism is contained within linear theory, and that, to first order, the period is set by linear processes. The main role of the nonlinearities appears to be to limit the growth of the oscillations.

It is worth noting from section 2c that we anticipate that near the reference basic state the growth rate of the coupled system will be generally comparable to the growth rate of the local instability, and the e-folding time for this growth is larger than the period of the resultant oscillations. In terms of the analysis of section 2, $\sigma_r\tau$ is comparable to c, and $\sigma_i^{-1} < \sigma_r/2\pi$. Hence for wind perturbations of realistic amplitude the coupled system will quickly reach a state where nonlinearities are important, and the theory of section 2 will not directly apply. The important nonlinear process is identified in section 4a.

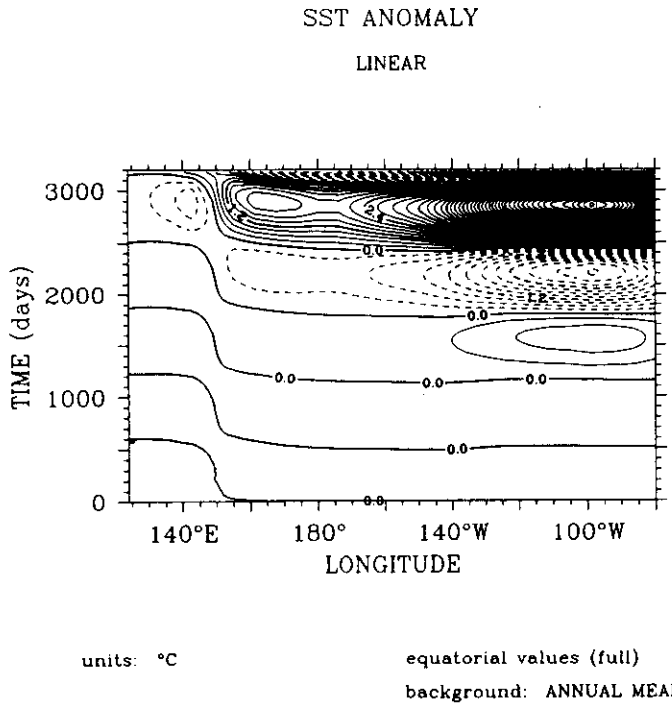

FIG. 4. Evolution of equatorial SST anomaly field (averaged between 2°N and 2°S) for the full linear model. SST anomaly has units °C.

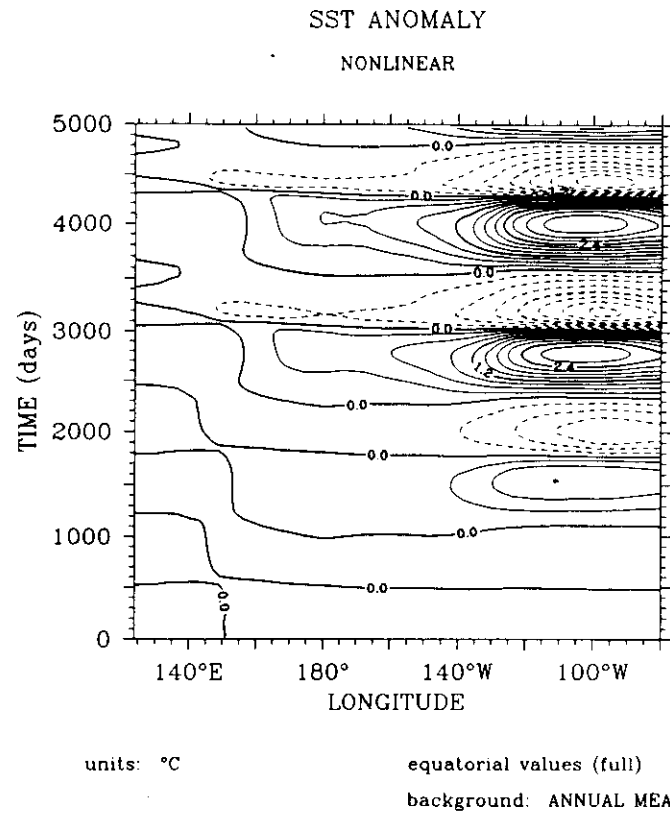

FIG. 5. Evolution of equatorial SST anomaly field for the full nonlinear model. SST anomaly has units °C.

a. The effects of remote wave processes on the interannual variability displayed by the coupled system

The strength of the equatorial Kelvin waves emanating from the western boundary reflection of the Rossby waves forced earlier in the eastern basin is represented by the parameter b in the simple analog model. We now consider the effects of an ocean medium that affords either larger kinetic damping of the waves, or an ocean geometry of basic state that reduces the amplitude of the returning Kelvin waves. This is done in the full numerical model by reducing the reflection efficiency of the Rossby mass flux incident on the western boundary;[1] the reference state and ocean geometry

[1] The formulation of the ocean model is such that the amplitude of the Kelvin mode generated by western boundary reflection is explicitly calculated (see Cane and Patton 1984). At the frequencies of interest, the amplitude of the Kelvin mode at the western boundary is proportional to the western boundary reflection efficiency.

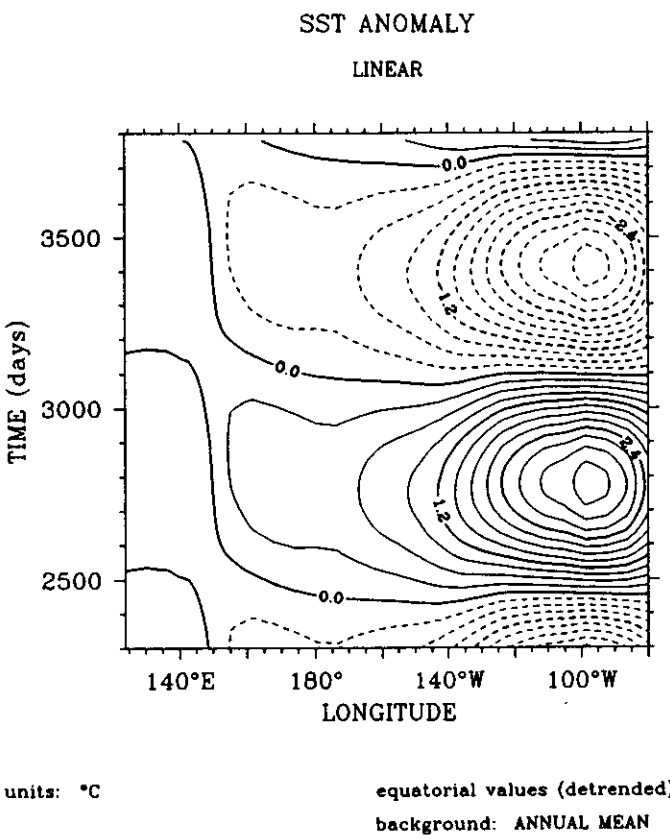

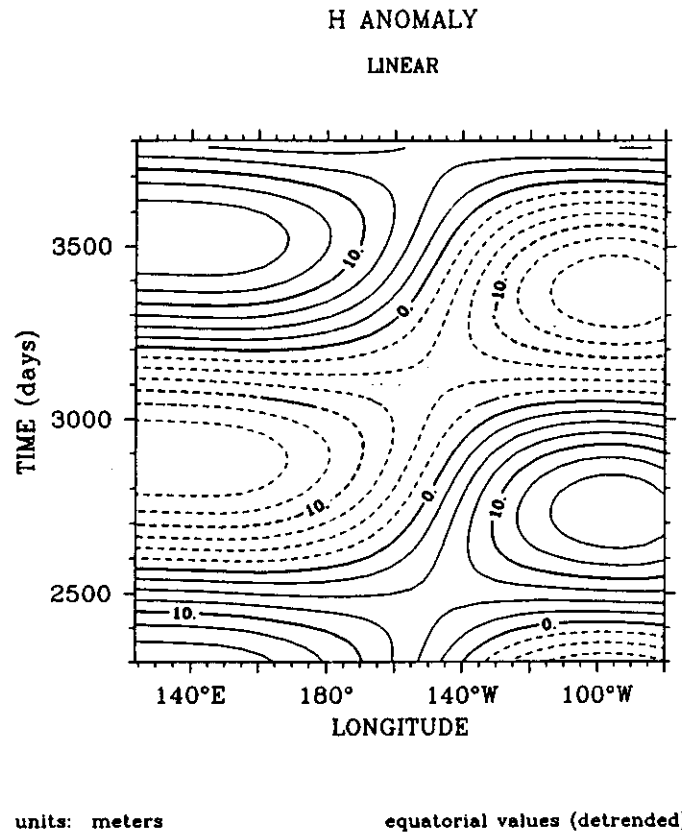

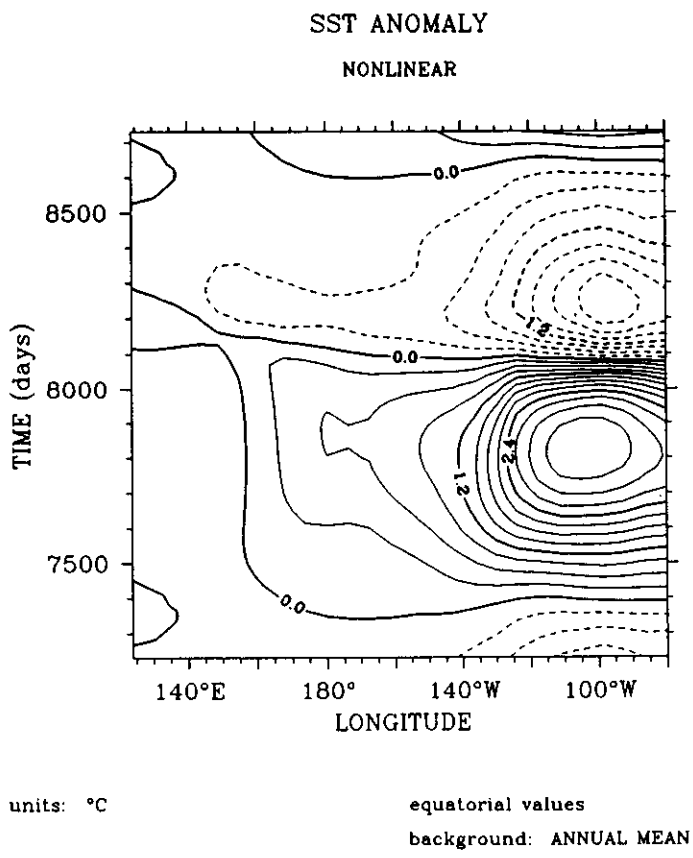

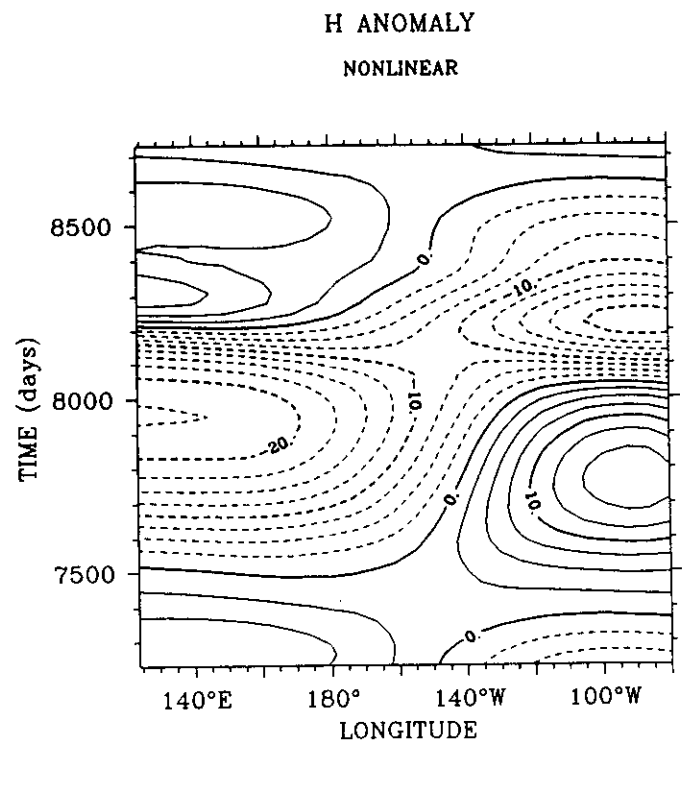

FIG. 6. Evolution of equatorial SST anomaly between the indicated times for (a) the full linear model where the overall exponential growth has been removed, and (b) the nonlinear model. Units are °C.

FIG. 7. As in Fig. 6, but for thermocline depth h (in meters).

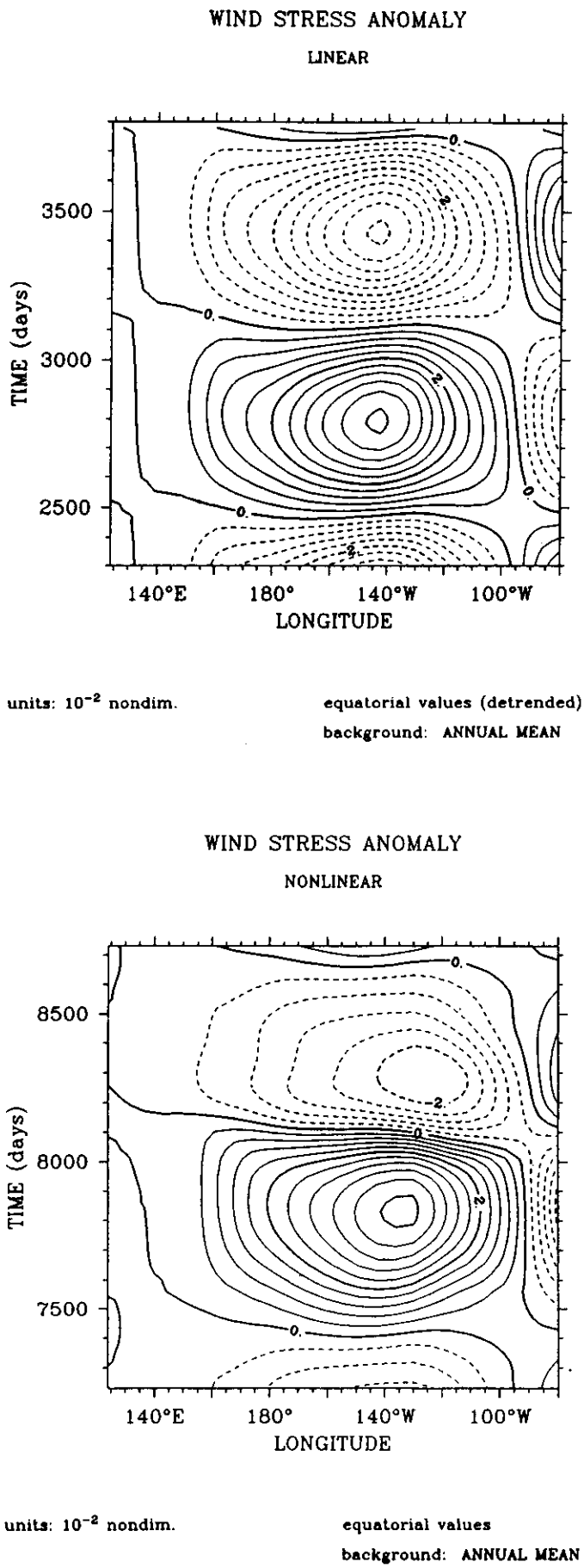

FIG. 8. As in Fig. 6, but for zonal wind stress (in N m^{-2}).

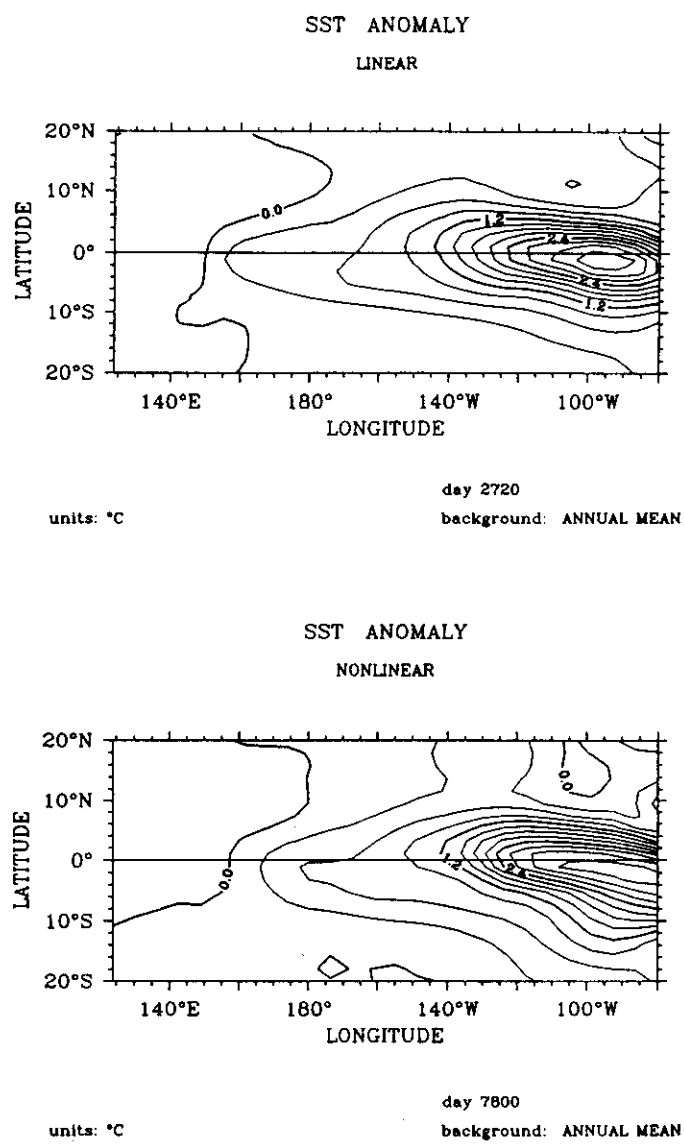

FIG. 9. SST anomaly fields for (a) linear and (b) nonlinear models at the indicated times, near the peak of a warm phase. Contour interval is 0.3°C.

are otherwise left unchanged. The results of these experiments are summarized in Fig. 10, along with estimates derived from the analog model as b is varied while c and τ are set at the reference values ($c = 2.2$ yr^{-1}, $\tau = 0.5$ yr). By reducing the strength of the reflected signal in the linear and nonlinear numerical models, the growth rate of the coupled system decreases, as long as the system is oscillatory. This result is somewhat surprising, but is in qualitative agreement with the simple analog model as b is decreased. (For a further discussion on growth rate as a function of b, see appendix A.) Decreasing the remote wave amplitude increases the period of the oscillations in the numerical models, a result also supported by the analog model. By reducing the remote wave amplitude by more than about 55%, the coupled system can no longer support periodic solutions. The growth rate of

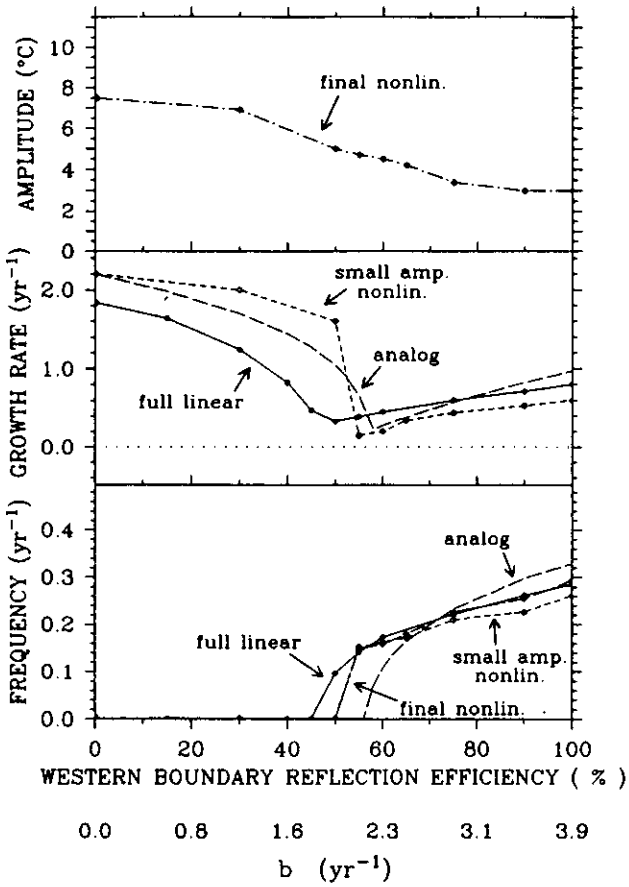

FIG. 10. Growth rate and frequency for the coupled models as a function of the strength of the remote wave signal (b). Each curve denotes a different model: the linearized full coupled atmosphere–ocean model (solid line), small amplitude (short dashed line) and final state (dashed-dot line) nonlinear full coupled model, and the analog model [Eq. (2.1); long dashed line]. The amplitude of the final state nonlinear oscillations is displayed in the top panel.

the system increases dramatically and, as $b \to 0$, is approximately the growth rate specified by the local instability process[2], $\sigma_r = c = 2.2\ \mathrm{yr}^{-1}$. Again, the transition point to pure growth solutions in the linear and nonlinear numerical models is in agreement with the analog model.

b. *Sensitivity of the variability of the coupled system to the local growth rate*

We explore this effects of changing the local growth rate in the simplest manner: changing the thermal dissipation time α_S^{-1} of the ocean. In addition to the reference value $\alpha_S^{-1} = 125$ days, we have made model runs with damping times ranging from 60 days to infinity (no thermal damping). Note, changing α_S has no effect on the remote wave processes. These results are displayed in Fig. 11, along with the estimates derived from the analog model as c is varied while b and τ are set at reference values. The qualitative agreement between the full model results and the simple model calculations is good. By increasing (decreasing) the thermal dissipation rate, the frequency of the oscillations increases (decreases). For small amplitude oscillations in the nonlinear and fully linearized models, the growth rates estimated from the numerical models are close to that calculated by the analog model, with larger (smaller) thermal damping rates α_S less (more) supportive of growth in the coupled system.

In decreasing the damping α_S, the linear, nonlinear and analog models undergo a transition from oscillatory, growing solutions to pure exponential growth. At large amplitude in the nonlinear model, oscillating solutions are obtained (Fig. 11) with small values of α_S. These events are now significantly modified by the nonlinearities associated with horizontal advection of SST rather than upwelling. The structure and evolution of these super model ENSO events becomes dissimilar

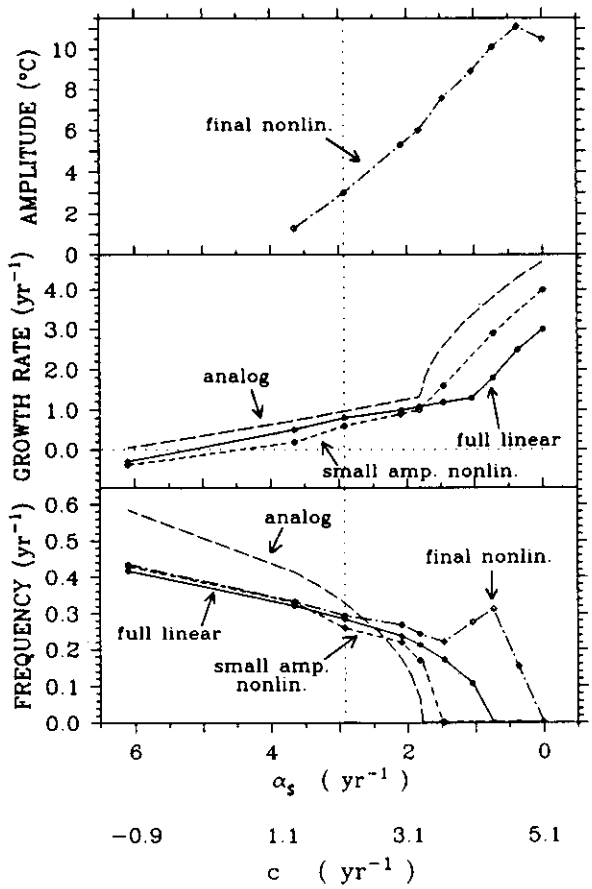

FIG. 11. Behavior of the coupled models as a function of the strength of the local instability processes (c). The vertical dotted line denotes the reference value for c, 2.2 yr^{-1}. Curves are as in Fig. 10.

[2] The small amplitude growth rates plotted in Figs. 10–13 for the oscillatory nonlinear solutions are those from peak of warm event to peak of the next warm event, or likewise from cold event to cold event. Such provides an overall growth rate for the coupled system; the growth rate into a warm event is somewhat larger than into a cold event due to a kink in the T_s profile at $h = 0$ [see Eq. (4.2) and appendix B]. The small amplitude growth rates for zero frequency solutions, however, are those for warming events and thus represent the maximum coupled growth rate.

to that assumed in the analog model, which no longer contains the essential physics for these large, unrealistic ENSO events.

c. *The effects of the time lag τ on the variability in the coupled system*

An increase in the longitudinal extent of the ocean domain, or the speed that the ocean waves propagate will change the time lag τ associated with the wave-induced processes b. Some full model runs are made with various size basins to examine the sensitivity of the coupled model interannual variability to τ. This is done by extending the ocean basin westward, and setting windstress and atmospheric heating to zero over this ocean extension. We have also reduced the ocean kinetic damping rate to $(250\ \text{yr})^{-1}$ to ensure a constant b. Since there are insignificant changes in SST in the model west of about 160°E, we retain the horizontal structure in the coupled model solutions, and effectively have only increased τ, leaving remote wave strength and local instability growth rate unchanged. The results of these experiments are displayed in Fig. 12. Increasing the time lag τ allows the system more time to grow through local instability processes (c) before the moderating remote wave processes (b) can act. Hence the period and growth rate of the resultant variability increases with increasing τ. At very large τ in the full linear model, solutions feature pure exponential growth ($\tau > 1.2$ yr; or a basin size twice the size of the Pacific). The "small amplitude" regime of the full nonlinear model also displays pure growth at approximately the local growth rate c, whereas the nonlinear full model oscillates at large amplitude because nonlinearity in the system does not allow unchecked growth. In these global-size ocean basins nonlinearity stabilizes the localized growing event in the eastern Pacific prior to the arrival of the remote waves. The remote signal does eventually enter the eastern basin, assuring the coupled system will oscillate. The resulting oscillation, however, appears very unrealistic, featuring very large amplitudes and long warm events separated by abrupt, brief cold events. The reader is refered to section 4 for further discussion.

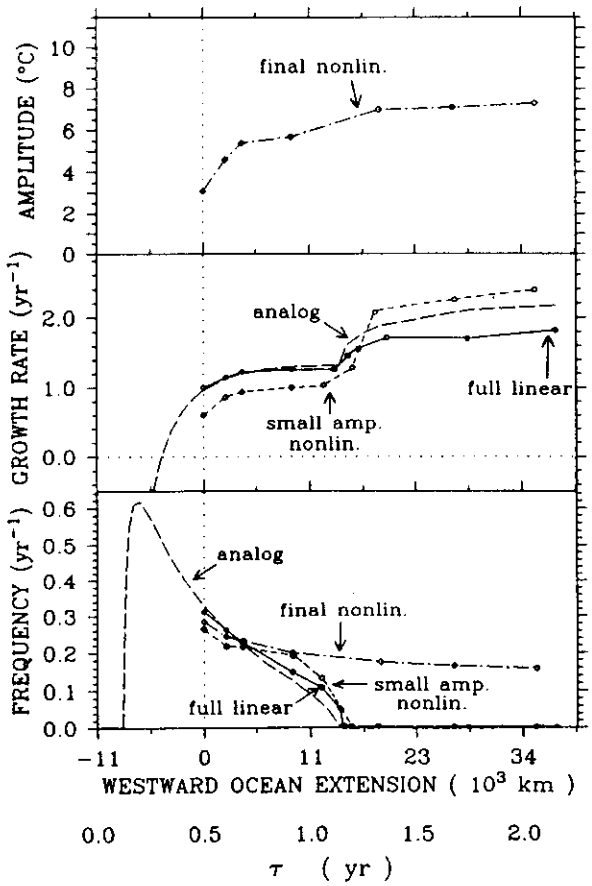

FIG. 12. Behavior of the coupled models as a function of τ, the wave transit time (see text). The vertical dotted line denotes the reference value for τ, 180 days. Curves are as in Fig. 10.

d. *Model behavior under reference states from different seasons*

There has been considerable speculation about the variation in the degree of coupled ocean–atmosphere instability during the annual cycle (e.g., Philander et al. 1984; Cane and Zebiak 1985; Hirst 1986; B88). Here we address the issue by running the full models with reference states that represent perpetual January–February, March–April, . . . , November–December climatic conditions, as obtained from the annual cycle used in B88. In each case, the full linear solution displays oscillations that grow with time. Growth rates and frequencies are shown in Fig. 13; growth rates are largest for July–August and smallest for November–December and January–February. Periods are in the range 3–5 yr. The full nonlinear solutions also display oscillations which, with the exception of the January–February case, grow until amplitudes given in Fig. 13 are reached. The small amplitude growth rates are similar to, or slightly less than, the corresponding linear model growth rates. The nonlinear January–February solution features an oscillation which slowly decays.[3] Periods for the nonlinear solutions are very similar to those for the corresponding linear solutions. Clearly, the background state is unstable with respect to small amplitude perturbations during most of the seasonal cycle.

The characteristics of the oscillation in each case broadly resemble that for the annual mean, with SST anomalies developing and decaying in situ and reaching largest magnitudes in the eastern basin. The retarded-oscillator mechanism is again responsible for the os-

[3] This apparent discrepancy between the linearized and small amplitude numerical model is primarily due to the kink in the $T_s(a(\bar{h}))$ profile at $h = 0$ [see Eq. (4.2)], which introduces nonlinear effects at small amplitude. These nonlinear effects are most prominent when mean upwelling is the weakest (early boreal spring).

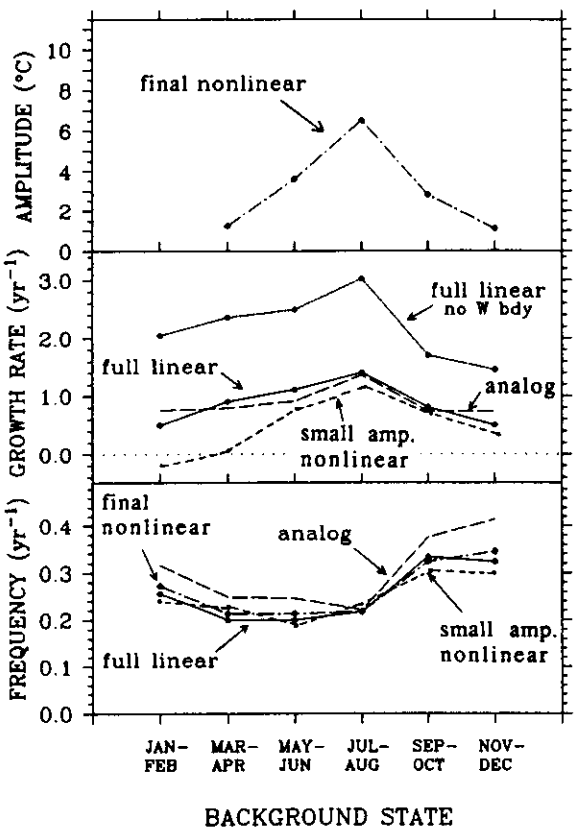

FIG. 13. The growth rate and frequency as a function of the two-month averaged basic state. The long dashed curve is for the analog model and the solid curve for the linear numerical model. The short dashed curve is for the full nonlinear model at small amplitude. The dash–dot curve for the fully nonlinear model at final state oscillation. The dotted curve denotes linear model growth rate in the absence of western boundary reflection.

cillations; setting the western-boundary reflection efficiency to zero leads in each case to pure exponential growth in the linear model and growth to some rather large perpetual warm state in the nonlinear model. The linear model growth rates so obtained are shown Fig. 13, and may be considered a measure of "local instability" c. Such growth rates are much larger than those for solutions when western boundary reflections are permitted, but otherwise display a similar seasonal pattern.

In order to gain some insight into the seasonal variation of local instability, the ocean thermodynamics for each of the no-west-boundary linear solutions are decomposed to yield values for the parameters listed in Table 1 for basic states given by the two month averaged fields, January–February, March–April, etc. The box 2°N to 2°S, 180° to 80°W is used for spatial averages of the various ratios (γ, β, π_i's). The ratios remain constant with time because of the pure exponential growth, hence no correlation analysis is necessary. We define $K_A^* = \langle \bar{u}T_x + \bar{v}T_y + \bar{T}_x u + \bar{T}_y v \rangle / \langle T \rangle$; K_A^* gives a more accurate representation of the contribution of advective processes to local instability than does the heuristic K_A of section 2a. To calculate a_L ($=\langle h_L \rangle / \langle \tau^x \rangle$), we use for h_L the model determined h field. Finally, we define the local instability growth rate

$$c = \beta a_L K + \beta \gamma K_E + K_A^* - \hat{K} - \alpha_s$$

[note that our use of the no-west-boundary linear solutions to define the various ratios guarantees that values of c are identical to the (pure exponential) growth rates of those solutions and introduces some variation in the analog model coefficients from those obtained in section 2 with the fully nonlinear model].

Figures 14 and 15 show the variation with season of various parameters important in the determination of local instability growth rate. It can be seen that while individual parameters undergo pronounced annual cycles, these fluctuations partly cancel to leave only relatively small changes in c. A comparison between March–April and July–August conditions provides illustration. Relative to July–August, the March–April background state features weak equatorial upwelling (small K) and weak SST gradients and surface currents (depressed K_A^*). The relatively weak equatorial upwelling in March–April results, however, in weakened thermal damping (small $\hat{K}$). Also, the band of equatorial convergence lies close to, or over, the equator in March–April, and convergence feedback is effective in

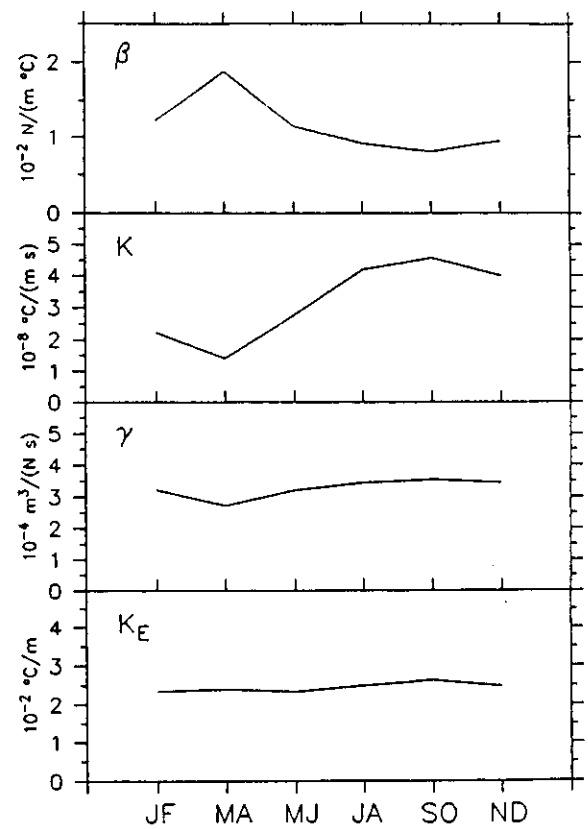

FIG. 14. Values of quantities important in the calculation of the analog model parameter c (β, K, γ and K_E) calculated for the six different background states based on two-month seasonal average fields (JF = January–February, etc.) from the no-western-boundary, linearized coupled numerical model.

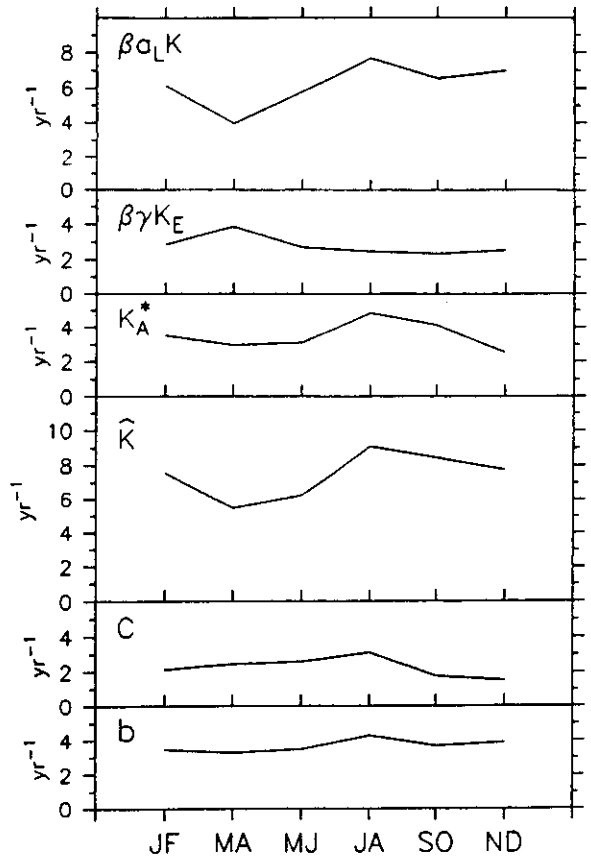

FIG. 15. As for Fig. 10, except for $\beta a_L K$, $\beta\gamma K_E$, K^*, $\hat{K}_A$. Also shown are the resulting values for c and b.

enhancing the atmospheric response to a given SST; consequently β is large. In July–August, the background atmospheric convergence zone lies well north of the equator, and β is small (see also Philander et al. 1984). In net, the local instability growth rates for March–April and July–August are not very different (see Fig. 15).

Finally, we investigate the behavior of the analog model when the parameters b and c are given values appropriate to each of the six seasonal states. We set c equal to the no-west-boundary growth rate for the linear model and calculate b as per section 2 using the respective value of β and the respective background field $\bar{w}$, and $a_W = 490$ m^3 N^{-1}. The values of b and c are shown in Fig. 15; τ has the value 0.5 yr throughout. Growth rates and frequencies of the resulting analog solutions are shown in Fig. 13. In each case, the value of b is large enough for the analog model to oscillate. Further, the variation in analog frequency somewhat resembles that for the full models. The analog frequencies tend to be too high, though, as for the annual-mean background. The analog growth rates are much reduced from the respective local instability growth rates, and have magnitudes comparable to those for the full linear model with total west-boundary reflection.

4. Nonlinear analog models

In this section we will identify the leading order nonlinearity in the full coupled numerical model which was used to derive the linear-delayed oscillator analog model in section 2 and perform the experiments described in section 3. We will derive the nonlinear analog model appropriate for the full numerical model which, in its simplest form, is contrasted to the nonlinear delayed oscillator model for ENSO postulated by Schopf (1987) and Suarez and Schopf (1988). We will show that nonlinearity in the full numerical model primarily acts to bound the amplitude of the oscillations, while the fundamental frequency (and growth rate) of ENSO events is determined by linear processes.

a. The nonlinear processes

The full coupled model behavior is, in general, characterized by finite amplitude oscillations. The period associated with the final state oscillations is typically 15% shorter than that observed in the initial stages of integration, when the system is well described by the linear full model equations. In all three sets of experiments, 3a–c, the changes in final state oscillation periods are in the same sense as that in the small amplitude regime of the full model, and predicted by the analog model. However, the final state solution is indeed nonlinear. When the full coupled atmosphere–ocean model is fully linearized, unbounded growth must and does occur.

There are three sources of nonlinearities in the coupled model: (i) the forcing of the atmosphere is a nonlinear function of the surface moisture convergence, (ii) the wind stress forcing of the ocean is a quadratic function of surface wind velocity, and (iii) the ocean SST anomaly depends on nonlinear horizontal advection terms and nonlinear vertical upwelling/mixing processes. A series of experiments have been run with the full model and various basic states that all lead to the following conclusions. The essential nonlinearity that moderates the exponential growth of the linearized system is the vertical upwelling processes that affect SST. Simply stated, the first limits on the amplitude of the growing coupled instability are set by the finite rate the ocean can cool or warm through changes in the pycnocline depth and the total upwelling rate. The nonlinearities associated with the forcing of the atmosphere, wind stress formulation and oceanic horizontal advection terms are not responsible for limiting the coupled atmosphere–ocean solutions. By eliminating each of these nonlinearities, in any combination, we obtain finite amplitude solutions. As long as the nonlinearity associated with vertical upwelling is retained, the solutions agree quantitatively with the solutions using the fully nonlinear model. Whenever this nonlinearity is eliminated, the final state oscillations display amplitudes that are unrealistically large.

b. The nonlinear analog models

In this section we will derive the nonlinear oscillator model based on the limiting nonlinearity in the full coupled model: the finite rate of heating of the surface layer through the pycnocline perturbations. This nonlinearity is captured in the parameterization of the subsurface temperature anomaly, T_s. In the model, the heating rate due to this term is [see Eq. (2.1)]

$$-\delta\Delta(\bar{w})\frac{\partial T}{\partial z} = -\delta\Delta(\bar{w})\frac{T - T_s}{H_1}; \qquad (4.1)$$

T_s is parameterized in terms of the pycnocline depth

$$T_s = \Theta(h)[\tanh(\lambda(\bar{h} + 1.5|h|)) - \tanh(\lambda\bar{h})], \quad (4.2)$$

where $\Theta = 28°\text{K}$ and $\lambda^{-1} = 80$ m for $h > 0$, and $\Theta = -40°\text{K}$ and $\lambda^{-1} = 33$ m for $h \leq 0$. In (4.2), h is the pycnocline perturbation (overbar denotes a time mean). The expression for T_s is due to Cane and Zebiak (1985), with one slight modification, and results from fitting (4.2) to the observed thermal structure across the equatorial Pacific Ocean (for further discussion, see Zebiak 1986). The nonlinear function (4.2) is the limiting nonlinearity in the full model. Elimination of all nonlinearities except (4.2) in the full model yields similar results as in the complete calculation, whereas very different oscillations result if we remove only the nonlinearity (4.2) from the full model, e.g., final state temperature perturbations of about 9°C.

Using (4.2) as our expression for T_s, we can now go through the same procedure outlined in section 3, in which we obtained the simple linear oscillator. This yields the following equation describing the eastern Pacific averaged SST

$$\boxed{\frac{\partial T}{\partial t} = \tilde{c}T + \frac{\delta}{H_1}\langle\Delta(\bar{w})T_s\rangle}, \qquad (4.3)$$

where T_s is given by (4.2), h by (2.4) and

$$\tilde{c} \equiv K_E\gamma\beta + K_A - \hat{K} - \alpha_s = c - \beta a_L K \approx -3.8\ \text{yr}^{-1}.$$

To understand the moderating effects of the nonlinearity (4.2) on the simple linear-delayed oscillator system (2.9), we will first consider simpler forms of the nonlinearity, based on (4.2).

We can formally expand (4.2) in terms of the pycnocline anomaly about the mean depth $\bar{h}$. The discontinuity at $h = 0$ prevents this expansion in simple terms, however, and introduces a symmetric component in the expansion of T_s that is small compared to the asymmetric nonlinearities. These symmetric nonlinearities do not significantly change the response of the system, and will be ignored. Thus the expansion of (4.2) about $\bar{h}$ yields

$$T_s = a(\bar{h})h - e^*h^3 + O(h^5). \qquad (4.4)$$

The value for the coefficient e^* is obtained in appendix C, and is only a qualitative estimate for this crude two-box model. Truncation of the expansion of (4.2) at the cubic limits the magnitude of possible h perturbations we may consider to about 40 meters. Substituting the approximation (4.4) into (4.3), and using (2.4) and (2.5), we obtain a simple relevant nonlinear equation for T:

$$\frac{\partial T}{\partial t} = -\hat{K}T + K(-a_W\beta T(t-\tau) + a_L\beta T) + K_E\gamma\beta T + K_A T - \alpha_s T - \hat{K}e^*(\beta a_L)^3[T - rT(t-\tau)]^3, \qquad (4.5)$$

where $r = a_W/a_L$. Equation (4.5), with $e^* = 0$, is exactly the linear oscillator equation (2.8). Rearranging (4.5), we obtain the first order correction to the linear oscillator:

$$\boxed{\frac{\partial T}{\partial t} = -bT(t-\tau) + cT - e[T - rT(t-\tau)]^3}, \qquad (4.6)$$

where $e = \hat{K}(\beta a_L)^3e^*$. For the tropical eastern Pacific, $e \approx 0.07°\text{C}^{-2}\ \text{yr}^{-1}$ and $r = 0.66$. The $e = 0$ solution is the linear-delayed oscillator equation that has, in general, exponential, oscillating solutions. Hence in the small amplitude regime, we expect (4.6) to reproduce the linear oscillator results of section 3, and thus describe the small amplitude regime of the full coupled atmosphere–ocean model. We will find that the delayed cubic term is an important term in describing the quantitative behavior of the coupled atmosphere–ocean system *only when the system reaches full nonlinear amplitude* (final state).

It is useful to consider the behavior of (4.6) when the nonlinear damping depends only on the instantaneous temperature $T(t)$. Note that this is not a physically based assumption, since in the model the cubic nonlinearity results from h^3, and h is a function of the local and lagged temperature. Dropping the final lagged term in (4.6) yields

$$\boxed{\frac{\partial T}{\partial t} = -bT(t-\tau) + cT - eT^3}. \qquad (4.7)$$

We have now formed three equations to examine the nonlinear effects in the simple analog models for the coupled atmosphere–ocean system. With increasing complexity and accuracy, these are given in (4.7), (4.6) and (4.3). The solutions to these equations are discussed in the next section.

c. *The effect of nonlinearity in the delayed oscillator model*

The nature of the solutions to (4.7) depends on the values of the coefficients b, c, e, and τ. Schopf (1987) and Suarez and Schopf (1988, hereafter SS) have postulated (4.7) as a simple model of ENSO, with similar physical processes attached to each term. However, Schopf and SS assume the dominant balance in (4.7) is between the linear and nonlinear local instability terms, and delayed effects play a secondary role. Specifically, SS assume $b < c$ and $c > 0$ (denoted domain R_1), and examine the behavior of the oscillations for various parameter changes. With the values SS choose, they find the system oscillates between two stable outer solutions

$$T = \pm\left[\frac{c-b}{e}\right]^{1/2};$$

the La Niña and El Niño states, if you will. For this parameter range the presence of the cubic term is fundamental for oscillatory, finite amplitude solutions. Setting $e = 0$ in (4.7) with parameter range R_1, one obtains nonoscillatory, infinite growth solutions.

Evaluation of the full coupled atmosphere–ocean model yields $b = 3.9\ \text{yr}^{-1}$, $c = 2.2\ \text{yr}^{-1}$, $\tau = 180$ d, and $e = 0.07°\text{C}^{-2}\ \text{yr}^{-1}$. These values fall in a domain R_2, defined by $b > c$, where the essential physics and behavior of (4.7) is quite different than in the domain considered in SS. In this regime the fundamental physics describes a (linear) interaction between the local instability growth and the delayed wave effects; nonlinearity (T^3) plays a secondary role in the oscillations. As in R_1, the domain R_2 yields finite amplitude oscillations for $\tau \to \infty$. In the parameter range R_2, however, there are no steady outer solutions. The system oscillates about a single, unstable zero basic state. There are no permanent La Niña or El Niño states in R_2. Additionally, setting $e = 0$ in (4.7) still allows oscillatory growing solutions, albeit to infinite amplitude, as $\tau \to \infty$. In domain R_1, it is not possible to examine small amplitude oscillations over more than one cycle. In domain R_2, however, small amplitude solutions are possible. These are given by the linearized version of (4.7), which was found in section 3 to simulate the behavior of the full coupled atmosphere–ocean model. A more complete discussion of the linear regime in domain R_1 is presented in appendix A and SS.

We recall from section 3 that the primary effect of the nonlinearities in the full coupled model was to limit the final state oscillation amplitude T_0, and increase the frequency of the final state oscillations from the frequency measured in the small amplitude state (by about 10%). We will first analyze (4.7), the simplified form of (4.6) to obtain the qualitative effects of damping on the linear system, and then address the more appropriate nonlinearity (4.6), and finally (4.3), the most complete form of nonlinear damping in the model.

Analytic final state solutions to (4.7) can be obtained in the following manner. First we write T in terms of a harmonic solution $T = T_0 e^{\sigma t}$ where $\sigma = i\sigma_i$ is pure imaginary, and expand the T^3 term to obtain

$$T^3 = \frac{3}{4} T_0^2 T + \text{higher harmonics.}$$

Insertion into (4.7) yields, ignoring the higher harmonics,

$$\sigma = -be^{-\sigma\tau} + c^*, \tag{4.8}$$

where $c^* = c - 3eT_0^2/4$. Since we desire the final state solution, we seek the neutral growth solutions to (4.8), i.e., the solutions with $\text{Re}(\sigma) = 0$. Equating the real and imaginary parts of (4.8), we obtain

$$\sigma_i = b \sin(\sigma_i \tau) \tag{4.9a}$$

$$T_0 = \pm\left[\frac{4}{3e}(c - b\cos(\sigma_i\tau))\right]^{1/2}, \tag{4.9b}$$

where σ_i is the frequency of oscillation. The solution (4.9) to (4.7) is displayed in Figs. 16 and 17. It should be noted that (4.9) is a very accurate approximation to the solution of (4.7) in domain R_2 (less than 2% error in σ_i, T_0). In domain R_1, the oscillations tend to be more square wave-like (cf., SS): neglect of the higher harmonics in the expansion of T^3 is not possible. In domain R_2, the domain of the coupled atmosphere–ocean system, (4.9) is a very good approximation to the solution of (4.7).

The solution (4.9) in Figs. 16 and 17 is the nonlinear equivalent to the linear solutions displayed in Figs. 2 and 3. Now, the final state temperature T_0 is akin to the growth rate in the linear system. We note the following consistencies between the linear and nonlinear systems:

- For a given strength of remote effects b, the system growth rate (final temperature T_0) increases with increasing local growth rate c. For decreasing b at a constant c, the growth rate (T_0) in the coupled system decreases (cf., Figs. 2a and 16a).
- In domain R_2, positive growth solutions (nonzero final state amplitude T_0) are possible only for some minimum frequency σ_i that depends on values of both b and c, and is independent of the strength of the nonlinearity e.
- For a fixed local growth rate c, increasing the remote restoring effects b decreases the period of the oscillations (cf., Figs. 2b and 16b). The minimum c for oscillatory solutions ($c = c_{\text{crit}}$) decreases with increasing b. c_{crit} is independent of the strength of the nonlinearity e^*, as is the frequency of oscillations at c_{crit}. For any given b, however, as c increases from c_{crit}, the effect of the nonlinearities is to decrease the period of the os-

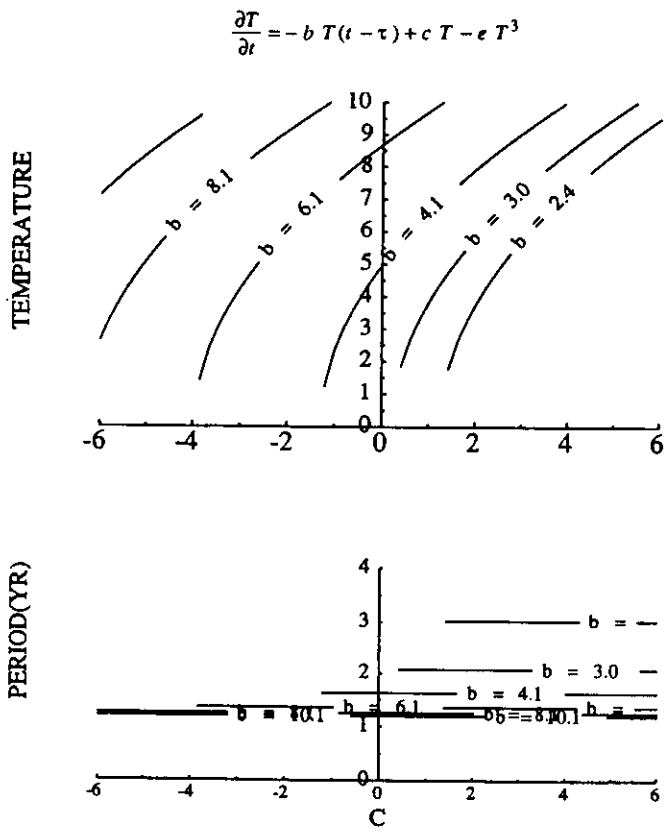

FIG. 16. The solutions to the delayed oscillator equation (4.7) with a reference value of τ = 180 days, and e = 0.07 C^{-2} yr^{-1}. The final state amplitude, T_0, of the system (in degrees C) vs the strength of the local instability term c is plotted in (a), and the period of the oscillation as a function of c is plotted in (b). Each curve represents a different value for b. Variables b and c are in units of yr^{-1}.

cillation from that obtained in the linear system to σ at c_{crit}.

- For set values of b and c, the growth rate of the oscillations (T_0) increases with increasing lag time τ. The cutoff lag time for oscillatory solutions in the linear solution is the same as in the nonlinear system (cf., Figs. 3a and 17a).
- For constant b, the period of the oscillation increases with increasing τ.

The behavior of the full model at the final state amplitude mimics that of both the small amplitude results in the full model, and the linear analog model in all three experiments of section 3 (Figs. 10–12). The solutions to Eq. (4.7) display the same qualitative behavior as the full model at final state amplitude except it does not allow the final state period to increase as c increases on a constant b (cf., Fig. 16b with Fig. 11). This result is due to neglecting the lagged component $T(t-\tau)$ in the cubic term of (4.6), and can be understood as follows. For small local growth rate c, the frequency of the linear oscillations is large (Fig. 2b) and $\sigma\tau$ is a large enough delay that $T - rT(t-\tau) \approx T$, and (4.7) is a good approximation to (4.6). However, as c increases, the wave effects take longer to overcome the local instability and the frequency of the linear oscillation decreases. As c gets very large, at large amplitude T the damping term is severely overestimated if the delayed term is ignored in the cubic [for $\sigma \to 0$, $T - rT(t-\tau) \to (1-r)T \approx 0.33T$]. Hence the nonlinear final state frequency calculated from (4.7) will be increasingly overestimated with increasing c.

A measure of the overestimation of the period shortening with increasing c is obtained by retaining the full nonlinear correction term to the linear oscillator [Eq. (4.6)]. Unfortunately, we could not find simple ana-

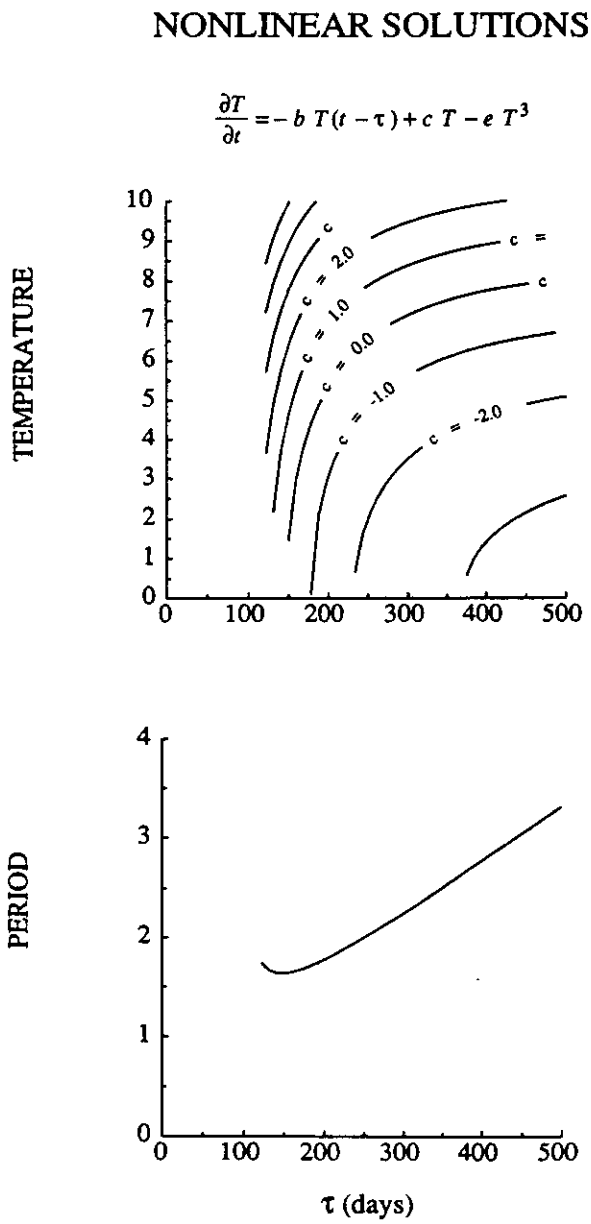

FIG. 17. The final state amplitude, T_0, (in °C) (a) and period (yr) (b) of the coupled system vs time lag τ, for b = 3.9 yr^{-1}, e = 0.07 C^{-2} yr^{-1}. Each curve is for a different reference value for c (in yr^{-1}).

NONLINEAR SOLUTIONS

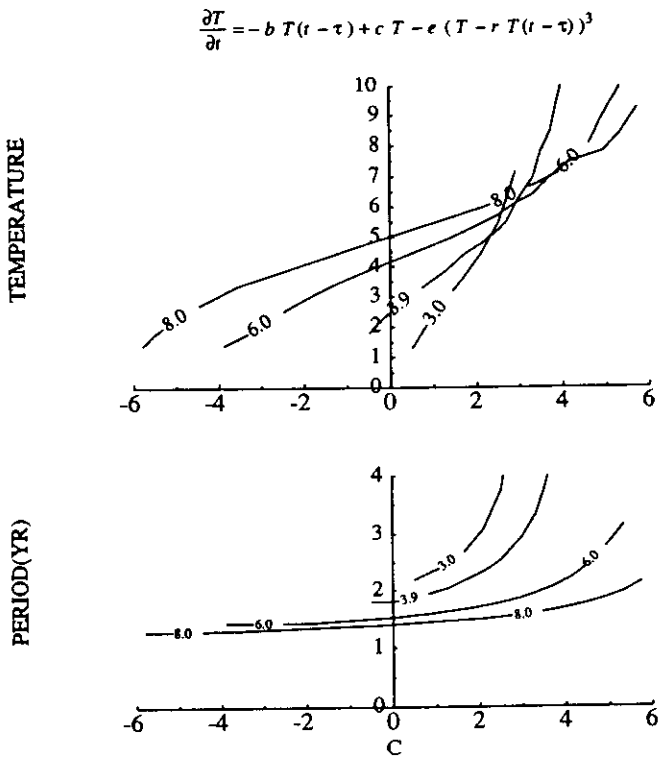

FIG. 18. Solutions for the delayed oscillator equation (4.6), with $r = 0.66$ (see Fig. 16).

lytic solutions to (4.6), as the higher harmonics are important in describing these oscillations. Equation (4.6) does have periodic solutions, although not sinusoidal. The nonzero finite amplitude solutions to (4.6) are obtained by numerical integration, and displayed in Fig. 18. The nature of the solutions to (4.6) are identical to that of (4.7), only now the final state period is indeed increased with increasing c, in agreement with the full numerical model results.[4] An example of the solution to (4.6) is displayed in Fig. 19 for the standard model derived values: $b = 3.9\ \text{yr}^{-1}$, $c = 2.2\ \text{yr}^{-1}$, $e = 0.07°\text{C}^{-2}\ \text{yr}^{-1}$, and with $r = 0.66$. The period of the oscillations (2.4 yr) has now increased from that obtained from the solution to (4.7) (1.7 yr), and the final temperature perturbations have decreased to 4.1°C from 7.5°C. We again note that, for the basic state b and c in the tropical Pacific, Eq. (4.6) does not exhibit steady outer solutions, but describes an unsteady oscillation about the mean (zero) state.

Finally, we would like to consider the complete form of the nonlinearity (4.2) in the simple model (4.3). Again, in (4.2) h is related to $\langle T \rangle$ through (2.4) and (2.5). Since we are interested in the qualitative behavior of (4.2), we have chosen $\bar{h}$ in (4.2) to be the value at the center of the eastern box (140°W, 0°N), and approximate (4.3) as:

$$\frac{\partial T}{\partial t} = \hat{c}T + \hat{K}T_s, \tag{4.10}$$

where $\hat{K}$ is defined in section 2.[5] The time lag is implicit in T_s {=funct[$h, h(t-\tau)$]}. The integration of (4.10) is displayed in Fig. 20 for the basic state Pacific coefficients. The three experiments done in section 3 with the full model and the simple analog model have been repeated with (4.10) (decreasing the reflection coefficient is equivalent to decreasing r), with similar results. Figure 20 is also useful, however, in explaining another aspect of the full coupled model solutions: the small time averaged warm temperature. This comes about primarily because of the asymmetry about the mean $\bar{h}$ of the nonlinearity in T_s. Since the depth of the mean thermocline increases from east to west on the equator, for a constant h perturbation along the equator the equatorial subsurface temperature changes will decay to the west. For the same h perturbation, with larger λ in (4.2), the subsurface temperature perturbations decrease in amplitude and are increasingly confined to the east. Therefore, the cold T_s anomalies ($h < 0$) are not as strong as the warm T_s produced by the equivalent positive h perturbation, hence the tendency for a net warm T in the full model. In the simple model (4.10), choosing $\bar{h}$ to be that at 140°W exaggerates this effect, since the subsurface cooling produced by pycnocline is only significant in the far eastern basin.

In conclusion, the limiting nonlinearity in the full coupled atmosphere–ocean model has been identified as the finite rate at which the upwelling processes can heat the surface layer. The primary effect of the nonlinearity is to bound the amplitude of the oscillations; the essential physics is contained in the linear oscillator equation, (2.9). The nonlinearities are not critical for oscillatory solutions, and account for only small corrections to the frequency from that in the linear, small amplitude oscillations. The form of this nonlinearity in the simple delayed oscillator model is derived. The nonlinear oscillator appropriate for our coupled atmosphere–ocean model does not have stable, steady solutions, but describes one bounded, unstable state, consistent with the linear results of section 3. In its simplest form, the nonlinear analog model is contrasted to that proposed by Schopf (1987) and SS. Although the physical processes invoked in these studies is similar to ours, the fundamental balance of terms is very different to what we find relevant for the coupled numerical model used in this study.

[4] Note the lines of constant b cross in the upper right hand corner of Fig. 18a because the curves for small b are now in region R_1.

[5] Formally, $\hat{K}$ includes the spatial correlation between $\bar{w}$ and T rather than between $\bar{w}$ and T_s. Within the box for averaging, however, T and T_s are relatively flat compared to $\bar{w}$. Thus, these correlations are very similar.

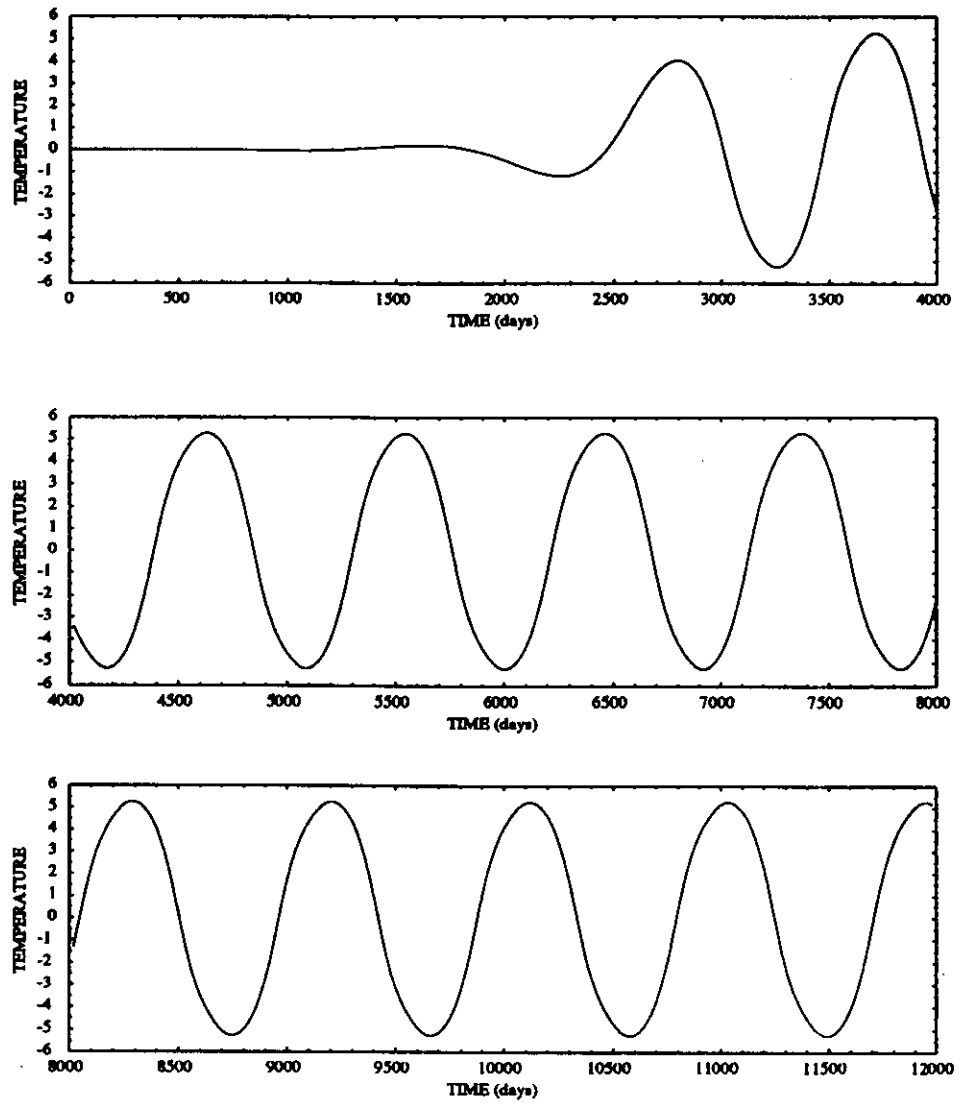

FIG. 19. Integration of (4.6) with the basic state values $b = 3.9\ \text{yr}^{-1}$, $c = 2.2\ \text{yr}^{-1}$, $e = 0.07\ \text{C}^{-2}\ \text{yr}^{-1}$, and $\tau = 180$ days. Temperature is plotted (in °C) vs time (days) for $r = 0.66$.

5. Conclusion and discussion

An analog model is developed to describe the nature of the interannual variability observed in the coupled atmosphere–ocean model with various basic state backgrounds for the ocean and atmosphere. The model is cast in terms of the sea surface temperature (SST) anomaly in an equatorial box (denoted T) in the eastern portion of the ocean basin, and includes all of the essential processes that regulate the SST in the equatorial eastern Pacific, identified by examing the full numerical model of the coupled tropical Pacific atmosphere–ocean system (see Battisti 1988a).

The analog model reduces to a linear-delayed oscillator equation for the SST averaged in the eastern equatorial Pacific,

$$\frac{\partial T}{\partial t} = -bT(t-\tau) + cT,$$

which has the solution of the form, $T = e^{\sigma t}$, where σ must satisfy

$$\sigma = -be^{-\sigma\tau} + c.$$

Here, t represents time, b the "remote" wave-induced processes that affect SST, τ a time lag, c the sum of the local instability processes acting in the eastern basin equatorial box, and $\sigma = \sigma_r + i\sigma_i$, where σ_r and σ_i are real, represent the growth rate and frequency of the coupled atmosphere–ocean system. The local processes c acting in the eastern basin give essentially instantaneous changes in T, and these local changes force changes in T of the opposite sense, delayed by a time τ. The local processes that set c are the following: changes in the SST due to horizontal advection, anomalous upwelling, ocean vertical thermal structure, and heat loss to the atmosphere. The remote process, b, results because, in the model, oceanic waves are forced

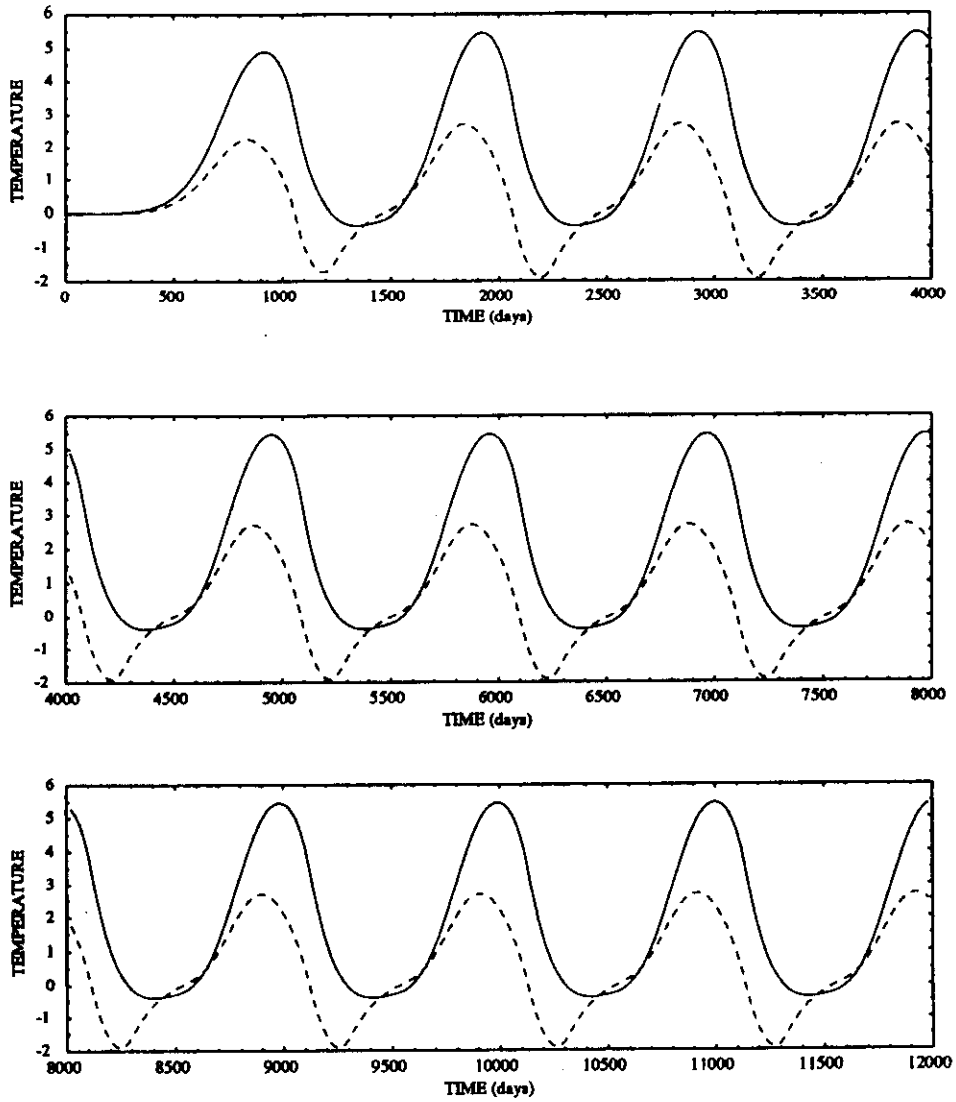

FIG. 20. Integration of (4.10) with the basic state values $\hat{c} = -3.9\ \text{yr}^{-1}$, $\hat{K} = 5.7\ \text{yr}^{-1}$, and $\tau = 180$ days. Temperature (in °Ç; solid curve) and thermocline perturbations (in tens of meters; dashed line) are plotted vs time (days) for $r = 0.66$.

in the eastern basin by (locally induced) changes in SST that in turn force wind stress anomalies. The wind stress anomalies, largely confined to the central and eastern basin, generate Rossby waves that propagate west and reflect off the western ocean boundary, generating Kelvin wave signal that enters the eastern basin at some time τ ($\approx$180 days) after the initial wave generation. The moderation of the local instability growth by these remote processes produces periodic oscillations with growth rates substantially slower than the coupled local instability $\sigma_r = c$.

This simple analog model, with values of b, c and τ representative of the tropical Pacific has a solution that is consistent with the fully nonlinear numerical model discussed in Battisti (1988a). In particular, the full and analog model display similar growth rates for the coupled system interannual variability to be 0.6 and 0.9 yr^{-1} respectively. The analog model estimates a period of oscillation at 3.0 yr, whereas the full nonlinear model displays interannual variability with a period of 3.4 yr. Finally, the analog model suggests the pycnocline changes should lead the SST changes in the eastern Pacific by about 65 days, compared to the full model result of 70 days.

We have used the analog model to predict the behavior of the interannual variability displayed in "basic states" that are somewhat different from that in the Pacific, the reference basic state. The behavior of the full numerical model with these new basic states is in qualitative agreement with that predicted from the simple analog model. Specifically, when the basic state is changed from the reference state so the local instability growth rate c is altered without changing the remote wave-induced processes, both models indicate that increases (decreases) in the local instability growth rate will substantially increase (decrease) the growth

rate and period of the interannual variability. For c large enough, no oscillatory solutions are possible and pure growth is supported. For c small enough, no growth is supported.

If the basic state changes are such that the local instability process and wave transit time remain at the reference values but the remote wave induced processes are reduced, the period of the resultant oscillations increases and, in a somewhat surprising result, the growth rate decreases. If b is sufficiently reduced in amplitude, no oscillations are possible and pure growth ensues. In the last set of experiments, we keep the strength of the processes b and c at the reference state values, and increase the basin width, hence the time lag τ. Increasing τ acts to increase both the growth rate and the period.

A central assumption made in the formulation of the simple analog model (2.9) and the use of a τ of 180 days is that the only significant west-boundary reflection in the full model is that of the gravest symmetric mode ($n = 1$) Rossby component. This possibility is certainly suggested by a decomposition of the full model oceanic fields into the various wave components which, in the case of the full linear model with annual-mean background, reveals that the $n = 1$, $n = 3$ and $n = 5$ Rossby reflections account for 77, 17 and 4 percent of the total Kelvin wave mass flux at the western boundary, respectively, while *all* the $n > 5$ Rossby reflections combined account for just the remaining 2 percent (see also Battisti 1988a). To more directly clarify the role of the $n = 1$ Rossby reflection, we have run the full linear model but allowed only the $n = 1$ Rossby reflection to contribute to the west-boundary Kelvin flux. The resulting oscillation is little changed from that in the complete reflection case, with a period of 3.6 yr, growth rate of 0.4 yr^{-1} and structure very similar to that in Fig. 9. In the converse experiment, where only the $n = 1$ Rossby reflection was excluded from contributing to the Kelvin mass flux, the solution features pure exponential growth. Thus the critical west boundary reflection is that of the $n = 1$ Rossby wave. The high n Rossby waves which take 2–4 yr to propagate across the ocean basin are also evident in the model solution, but the mass flux associated with these waves is too miniscule to influence the oscillation (cf. McCreary 1983).

The crucial nonlinearity in the full ocean model is due to the intrinsically limited ability of upwelling to generate SST anomalies. The nonlinear processes are secondary effects in the numerical model, and are shown to primarily bound the magnitude of the interannual variability in the coupled system and slightly increase (by about 10 percent) the frequency of the final state oscillations from the frequency at small amplitude. The characteristic small amplitude growth rates and the period of the interannual variability are set by the (mean) basic state of the atmosphere and ocean and are consistent with both the full model results (with or without the nonlinear processes) and the simple linear analog model. We derive the nonlinear analog model relevant for the ENSO events in the coupled numerical model, which reduces to a nonlinear delayed oscillator equation. This nonlinear analog model is similar in form to that proposed by Schopf (1987) and SS. The essential physical balance featured in these two models, however, is completely different. Both the linear and nonlinear delayed oscillator models we have derived characterize the coupled system as oscillatory about one unstable state: the mean state. The analog model results, in concert with the full coupled numerical model integrations, indicate steady, stable warm (El Niño) and cold (La Niña) states are not possible for the parameter regime of the Pacific.

In all of the experiments with different basic state oceans, the solution to the analog model correctly predicted the behavior of the fully coupled numerical atmosphere–ocean model. The success of the simple analog model allows us to speculate on two important aspects of the coupled atmosphere–ocean system, both of which involve the remote equatorial wave processes acting in the western basin. The first issue concerns the effects of the basin size on the nature of the interannual variability. From the analog model, we expect that ocean basins much narrower in longitude than about 13 000 km will not be able to support interannual variability analogous to ENSO. Although this calculation is valid for a fixed size eastern ocean box, using small eastern ocean boxes with the same basic state as for the eastern Pacific gives the same result. Hence the simple analog model indicates neither the tropical Indian or Atlantic Ocean should support interannual variability as described in the full numerical model.

Remote wave processes and western boundary reflection of these waves are crucial to this model ENSO cycle. In the western Pacific, the oceanic boundary is quite irregular and far from meridional. Additionally, it is not clear that the Rossby waves generated in the central/eastern Pacific will actually survive the trip to the western boundary in the presence of a vigorous undercurrent, although Bigg and Blundell (1988) have found evidence for the gravest mode symmetric Rossby wave propagation in the western Pacific prior to the 1982 ENSO event. Our calculations suggest that the same dynamical and thermodynamical processes acting to control the interannual variability in the idealized, full numerical model can still act to produce ENSO-like interannual variability, even if Kelvin waves that come from the western basin into the eastern Pacific are severely reduced in amplitude from the idealized situation.

Finally, we arrive at the question of predictability of interannual variability in the coupled system. All of our model calculations suggest that the basic state of the system is the most crucial factor in determining whether the coupled system will support growth

through local instability that leads to ENSO-like events. Hence, the question of predictability should depend, to a large extent, on specifying the basic state of the ocean and atmosphere. The time mean state of the Pacific atmosphere and ocean is supportive of growth. However, there are certainly times in the annual cycle (e.g., Northern Hemisphere winter) where, according to the simple model, conditions are not ideal for growth. During these times, the predictability of the variability of the coupled system should be at a minimum (see section 5 of Battisti 1988b). We are currently planning a series of experiments to examine the predictability of the interannual variability in the tropical Pacific.

The analog models we have derived from the full coupled numerical model contains the essential physics for ENSO events in the (Cane and Zebiak) numerical model. We suspect the essential physics which are responsible for ENSO events in these models are similar to those in the coupled numerical model of SS. In both models there is essentially a single mode of coupled atmosphere–ocean instability which is quasi-stationary, primarily because of the zonal asymmetry in the mean state (cf., the propagating instabilities described by Hirst 1986, 1988 for a zonally uniform mean state). We would like to emphasize the scenario for ENSO in these simple models has yet to be verified by observations. In addition, there are probably other modes of instability in nature which may successfully compete with the dominant quasi-stationary mode for ENSO found in these simplified coupled atmosphere–ocean models. We expect that by increasing the complexity of the coupled model (e.g., increasing vertical resolution in the ocean, explicitly modeling boundary-layer processes in the atmosphere) such modes will arise, and plan to examine these modes in future studies.

Acknowledgments. The authors would like to thank Dennis Hartmann, Ed Sarachik and Paul Schopf for the many stimulating conversations during the course of this work, and David Neelin for his valuable criticism on the manuscript. The authors would also like to thank Ed Harrison and Dennis Hartmann for the use of their computer systems. DSB was supported by Grants ATM-83-16233 and ATM-86-20077 from the National Science Foundation Climate Dynamics Program, Atmospheric Sciences Division, and a grant from the NOAA Equatorial Pacific Ocean Climate Study (EPOCS). ACH was supported by Grant NA-85-RABH-0031 from the Joint Institute for the Study of the Atmosphere and Oceans.

APPENDIX A

General Properties of the Linear-Delayed Oscillator

The equation

$$\frac{\partial T}{\partial t} = -bT(t-\tau) + cT \qquad \text{(A1)}$$

is a simple example of a class known as "differential delay equations." There exists an extensive literature on this class of equations (see Saaty 1981 for an introduction), although most treatments focus on nonlinear differential delay equations and associated chaotic behavior (e.g., May 1983). This section focuses on general properties of the linear equation (A1) which will be helpful in the comparison with the full model results presented in section 3.

As noted in section 2, solutions to (A1) with $b = 0$ are pure exponential with growth rate c. To determine the system's behavior at nonzero b, solutions of the form $T = T_0 \exp[\sigma t]$ are sought (σ may be complex). Permitted growth rates (σ_r) and angular frequencies (σ_i) are obtained from solution of the relation

$$\sigma = -be^{-\sigma\tau} + c. \qquad \text{(A2)}$$

The behavior of the system is illustrated in Fig. 21 for a range of b and c. When lagged negative feedback is weak ($0 < b < \exp[c\tau - 1]/\tau$), the fastest growing solution still displays pure exponential growth/decay, but with reduced growth rate. A second pure exponential solution possessing even lower growth rate also exists. At $b = \exp[c\tau - 1]/\tau$, the two exponential solutions become degenerate, here independent solutions are $T = T_0 \exp[\sigma t]$ and $T = T_0 t \exp[\sigma t]$; $\sigma = c - \tau^{-1}$. Note that, for the basic state Pacific variables ($c = 2.2\ \text{yr}^{-1}$, $b = 3.9\ \text{yr}^{-1}$ and $\tau = 180$ days) this range of solution is not relevant.

When lagged negative feedback is strong relative to the local growth processes ($b > \exp[c\tau - 1]/\tau$), solutions of (A1) are oscillations whose amplitudes grow or decay exponentially with time. In this oscillatory regime, it is illuminating to split (A2) into real and imaginary parts to get two equations for σ_r in terms of σ_i:

$$\sigma_r = c - \sigma_i/\tan(\sigma_i\tau) \qquad \text{(A3a)}$$

$$\sigma_r = \frac{1}{\tau}\ln\left[\frac{b\sin(\sigma_i\tau)}{\sigma_i}\right]. \qquad \text{(A3b)}$$

The intersection of (A3a) and (A3b) yield the permitted growth rates and frequencies. Equations (A3a) and (A3b) are plotted in Fig. 22, which shows that there exists a slowly oscillating solution of period ($2\pi/\sigma_i$) always greater than 2τ and a series of rapidly oscillating solutions having periods near $\tau/(n + \frac{1}{4})$, $n = 1, 2, 3, \cdots$. The high frequency solutions generally have high decay rates. Such solutions might have positive growth rates only if $b > (2n + \frac{1}{2})\pi/\tau$, i.e., at values very much larger than those relevant to the full model.

The slowly oscillating solution is the analytic continuation of the pure exponential solutions previously discussed; both growth rate σ_r and frequency σ_i increase rapidly as b increases, and σ_r is positive for the most

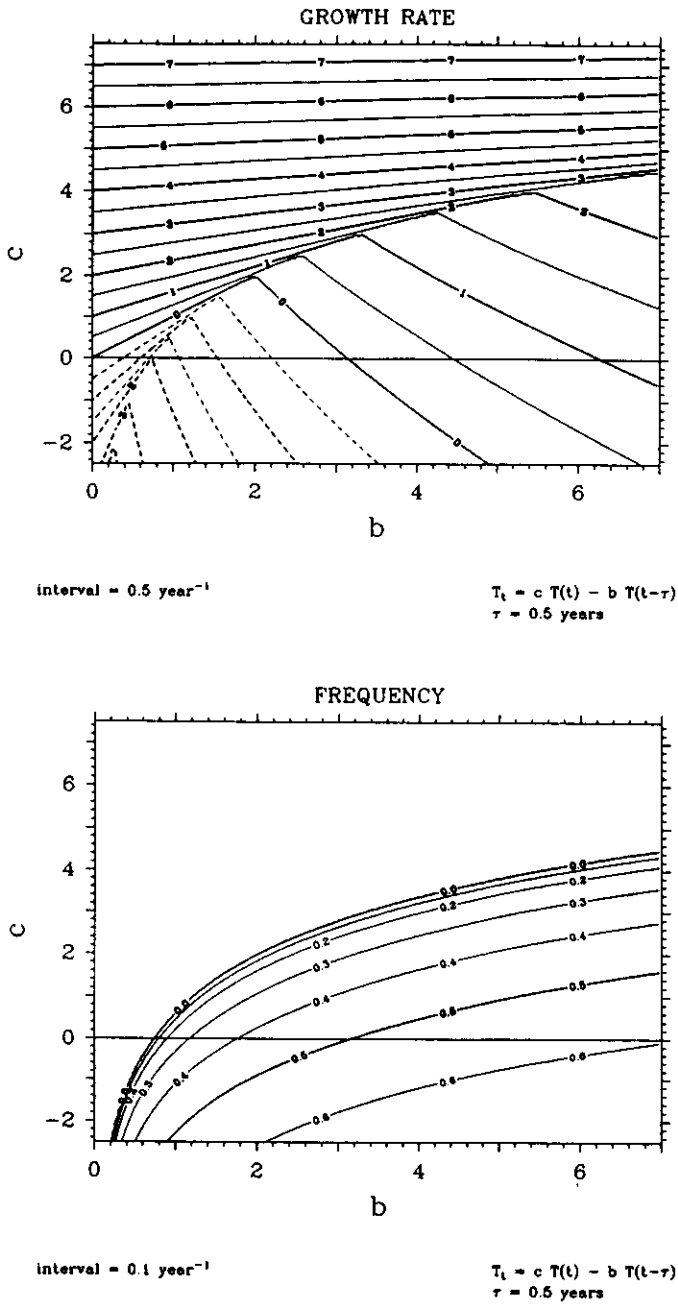

FIG. 21. Behavior of fastest growing solution to the delayed oscillator equation (A1): growth rate and frequency as b and c are varied while time delay τ is held at 180 days. Variables b and c have units yr^{-1}.

relevant parameter values. The condition for σ_r to be positive is approximately

$$b > \frac{\pi}{2\tau} - \left[\frac{\pi}{2} - 1\right]c. \qquad \text{(A4)}$$

The above condition holds exactly only at $c = \tau^{-1}$ and at $c = 0$, but is correct to within a few percent of the true critical b for the range $-1 < c < 2.1\ yr^{-1}$ in Fig. 21. [An exact, but implicit, formula for the critical b may be readily derived by setting $\sigma_r = 0$ in (A3a) and (A3b).]

It may seem curious that as the strength of the lagged negative feedback (i.e., b) is increased, the growth rate σ_r of the slow oscillation also increases, and may reach values much larger than that for local instability alone (i.e., c). It can be shown from (A3a) that $\sigma_r > c$ when the oscillation has period between 2τ and 4τ [i.e., when $b > \pi \exp[c\tau]/(2\tau)$. To understand the connection between period and growth rate, multiply (A1) by $T(t)$ to get

$$\frac{\partial T^2}{\partial t} = 2cT(t)^2 - 2bT(t)T(t-\tau). \qquad \text{(A5)}$$

The growth in T^2 from one maximum to the next depends on the local contribution $2c \int T(t)^2 dt$ (always of the same sign as c) and the lag contribution $-2b \int T(t)T(t-\tau)dt$. The lag contribution adds to growth when there is a negative correlation between $T(t)$ and $T(t-\tau)$. This can be shown to occur when $\pi/(2\tau) < \sigma_i < \pi/\tau$, i.e., when the period is between 2τ and 4τ. For illustration, consider the situation when σ_i approaches π/τ: $T(t-\tau) = T_0 \exp[\sigma_r(t-\tau)] \cos[\pi t/\tau - \pi]$ has sign almost always opposite that of $T(t) = T_0 \exp[\sigma_r t] \cos[\pi t/\tau]$, and so clearly $\int T(t)T(t-\tau)dt < 0$.

The effect of varying τ on the behavior of the fastest growing solution to (A1) is illustrated for ranges of b and c in Figs. 23 and 24. For parameter values relevant to the full model, σ_r is large negative when τ is very small (i.e., when the ocean basin is very narrow); here the effect of the time delay in (A1) is small and the (negative) growth rate is of the order $c - b$. As τ is increased, the growth rate increases towards a limit, which is equal to c when $c > 0$. The value of τ for neutrality [$\sigma_r = 0$] is given with an error of less than 5% by the approximate relation (A4), for the range $-1 < c - 4\ yr^{-1}$ and $1.5 < b < 10\ yr^{-1}$. The frequency

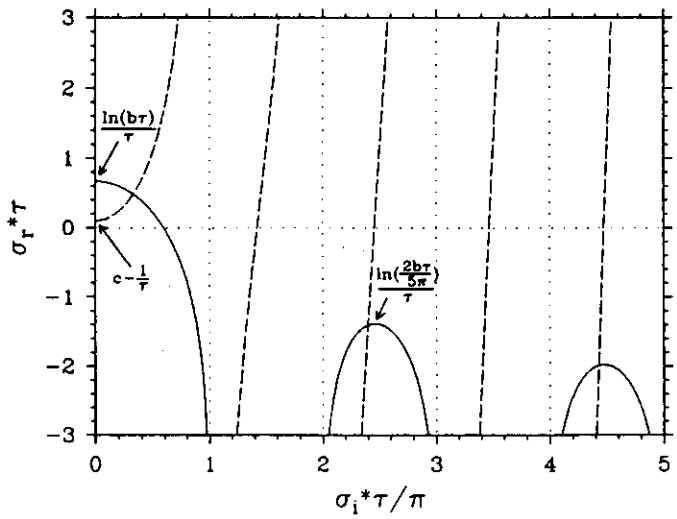

FIG. 22. Values of σ_r as given by (A3a) [dashed] and (A3b) [solid] versus angular frequency σ_i. The intersections indicate solutions to (A1). Units of the scaled variables are nondimensional.

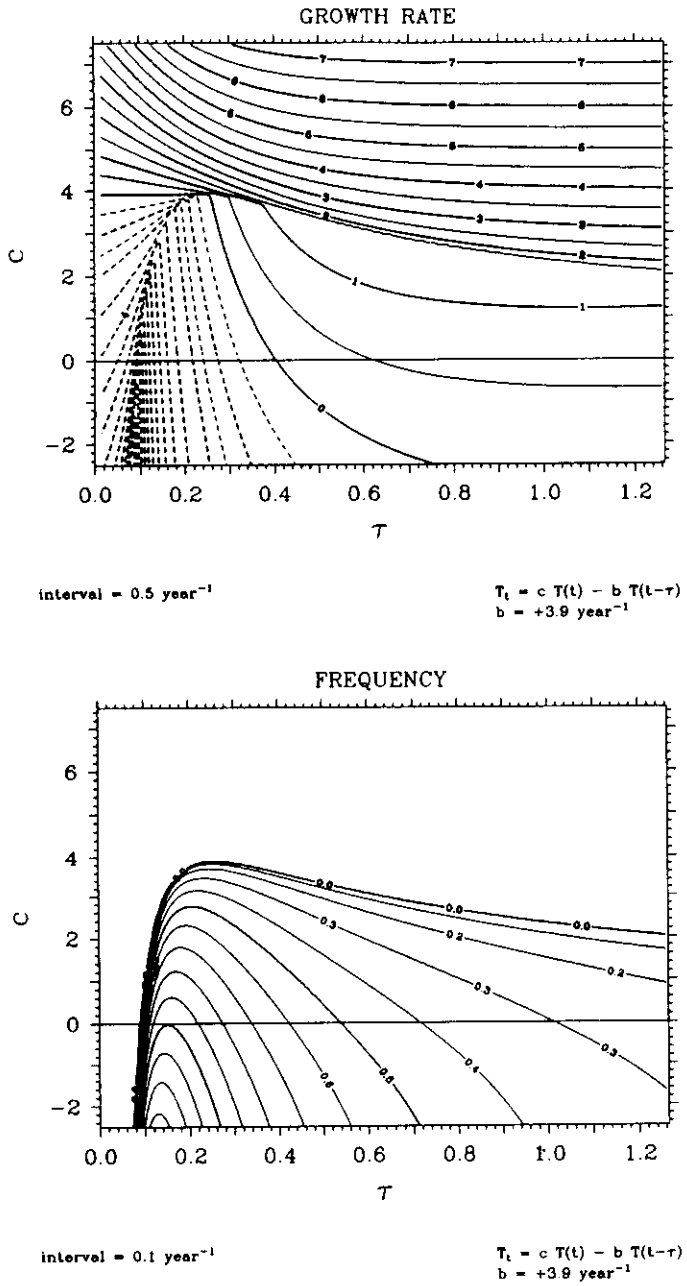

FIG. 23. Behavior of fastest growing solution to the delayed oscillator equation (A1): growth rate and frequency as c and τ are varied while delayed feedback coefficient b is held at 3.9 yr^{-1}. c has units yr^{-1}, τ has units yr.

generally decreases with increasing τ, for τ over 0.3 yr. At very large delays, the solution reverts to pure exponential growth, if $c > 0$.

APPENDIX B

Linearization of the Coupled Model

The derivation of the full linear model from the full nonlinear model of B88 is outlined here. Outside the SST anomaly equation, the "full nonlinear model" really features only two nonlinear processes: wind stress on the ocean and dependence of atmospheric heating on convergence. The nonlinear windstress on the ocean is

$$\tau^x = \rho_a C_D[|\bar{\mathbf{U}}_a + \mathbf{U}_a|(\bar{U}_a + U_a) - |\bar{\mathbf{U}}_a|\bar{U}_a]$$

$$\tau^y = \rho_a C_D[|\bar{\mathbf{U}}_a + \mathbf{U}_a|(\bar{V}_a + V_a) - |\bar{\mathbf{U}}_a|\bar{V}_a], \quad \text{(B1)}$$

where $\bar{\mathbf{U}}_a$ is the mean surface velocity ($\bar{\mathbf{U}}_a = \mathbf{i}U_a + \mathbf{j}V_a$). The complete linearized version of (B1) is then

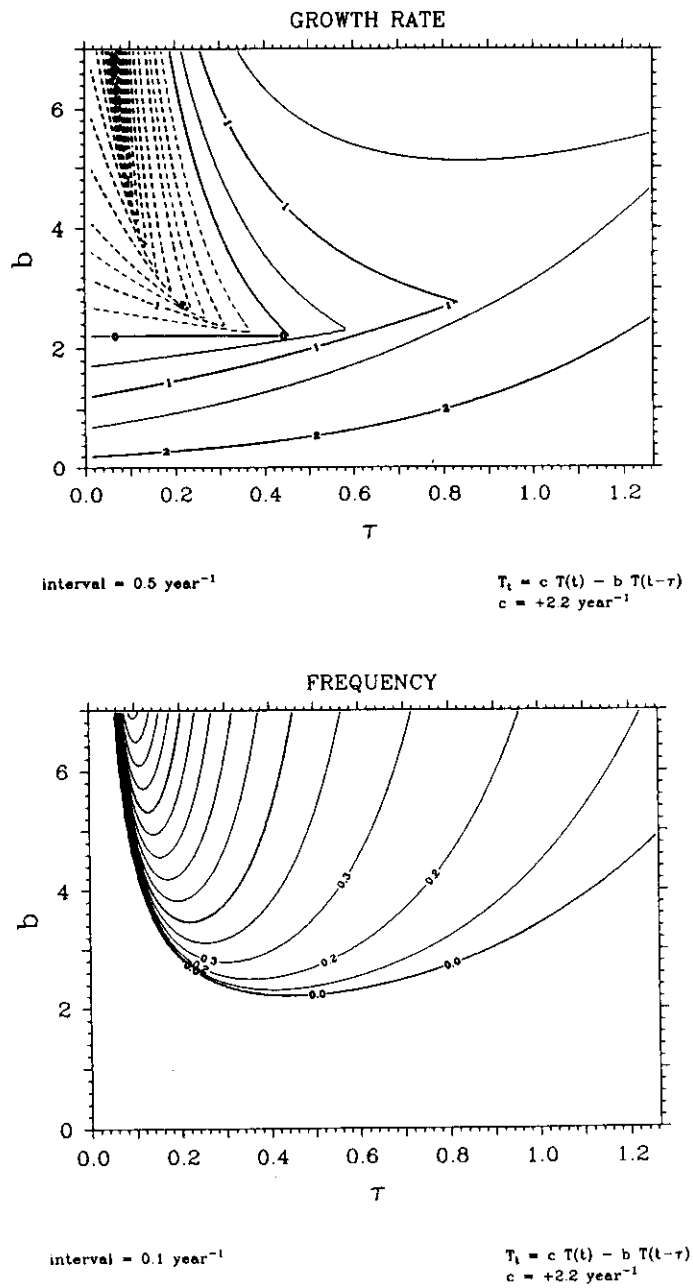

FIG. 24. Behavior of fastest growing solution to the delayed oscillator equation (A1): growth rate and frequency as b and τ are varied while local-instability growth-rate c is held at 2.2 yr^{-1}. b has units yr^{-1}, τ has units yr.

$$\tau^x = \rho_0 H_0 (K_s{}^x U_a + K_s{}^c V_a)$$
$$\tau^y = \rho_0 H_0 (K_s{}^y V_a + K_s{}^c U_a), \qquad \text{(B2)}$$

where

$$K_s{}^x = \frac{2\bar{U}^2 + \bar{V}^2}{(\bar{U}^2 + \bar{V}^2)^{1/2}} \frac{\rho_a C_D}{\rho_0 H_0} \quad K_s{}^y = \frac{\bar{U}^2 + 2\bar{V}^2}{(\bar{U}^2 + \bar{V}^2)^{1/2}} \frac{\rho_a C_D}{\rho_0 H_0}$$
$$K_s{}^c = \frac{\bar{U}\bar{V}}{(\bar{U}^2 + \bar{V}^2)^{1/2}} \frac{\rho_a C_D}{\rho_0 H_0}.$$

The atmospheric heating in the full nonlinear model given by B88 becomes in the linear (or small perturbation) regime,

$$Q = \alpha(\bar{T}) + \begin{cases} 0, & \nabla \cdot \overline{\mathbf{U}_a} > 0 \\ \beta^* \nabla \cdot \mathbf{U}_a, & \nabla \cdot \overline{\mathbf{U}_a} \leq 0. \end{cases} \qquad \text{(B3)}$$

Thus convergence feedback is restricted to regions where the reference state wind is convergent. Heating is calculated iteratively at each time step, using the part given by the SST anomaly field as first guess. The linearization of the SST anomaly equation has been discussed in section 2. The equation used in the full linear model is [cf., Eq. (2.1)]

$$\frac{\partial T}{\partial t} = -\mathbf{u} \cdot \nabla \bar{T} - \bar{\mathbf{u}} \cdot \nabla T - \delta H(\bar{w}) w \frac{\partial T}{\partial z} + K_T h - dT, \qquad \text{(B4)}$$

where

$$K_T = \frac{\delta \Delta(\bar{w}) a(\bar{h})}{H_1}, \quad d = \alpha_s + \delta \frac{\Delta(\bar{w})}{H_1}.$$

In other respects, the linear model conforms to that of B88.

All but one of the nonlinear processes in the full nonlinear model approach linearity in the small perturbation limit. The exception is in the expression for T_s, where, in the small perturbation limit,

$$T_s = \begin{cases} a^+(\bar{h})h, & h > 0 \\ a^-(\bar{h})h, & h \leq 0, \end{cases} \qquad \text{(B5)}$$

with $a^+(\bar{h})$ larger than $a^-(\bar{h})$ by typically a factor of two or more. Consequently, most of the growth of the small amplitude nonlinear solutions occurs during the warm phase. In the pure growth regimes of Figs. 10–12, the small amplitude warm solution (which follows a westerly wind burst initialization) has growth rate considerably larger than the linear model (where $a(\bar{h}) = (a^+(\bar{h}) + a^-(\bar{h}))/2$), while the small amplitude cold solution (following an easterly wind burst initialization) has smaller growth rate.

The annual mean and seasonal reference states feature fields of rich zonal and meridional structures, which is reflected in the horizontal structures of the

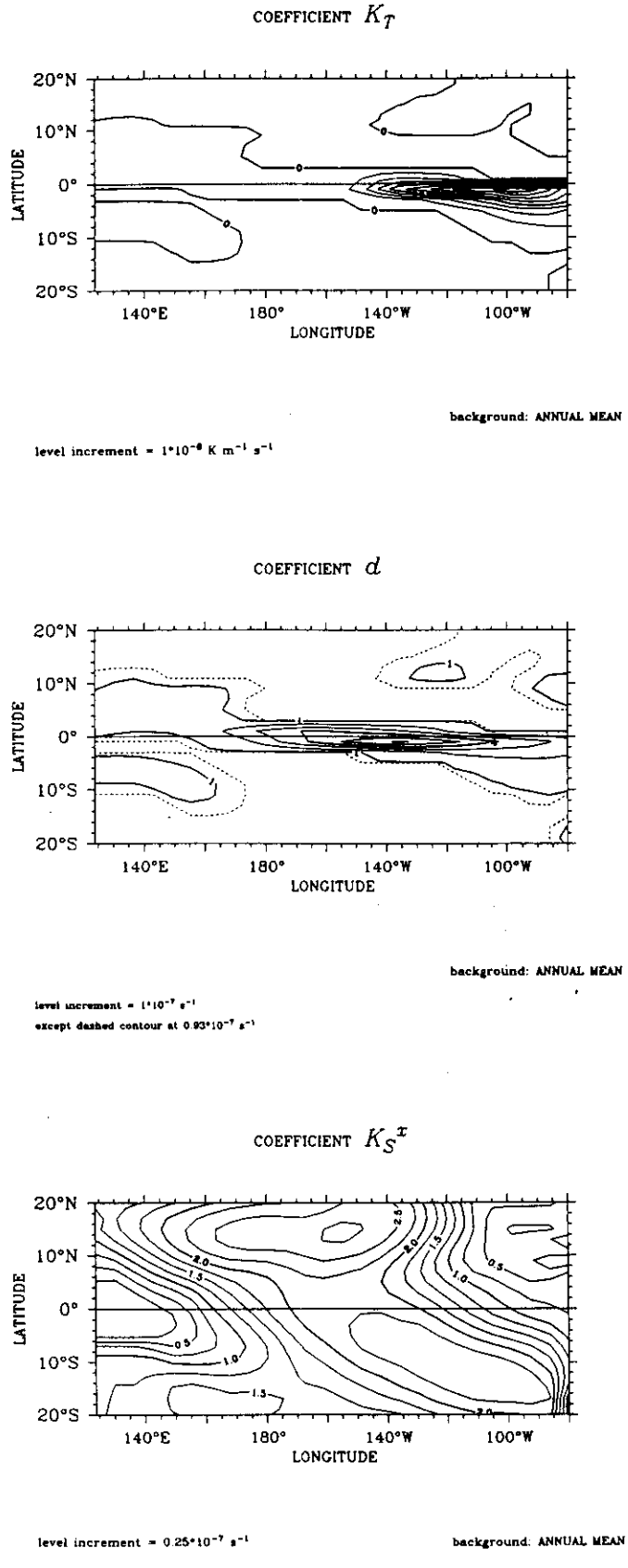

FIG. 25. Spatial structure of the ocean thermodynamic coefficients K_T and d and the zonal windstress coefficient $K_S{}^x$ as computed from the annual mean reference state. The contour intervals are as follows: K_T, 10^{-8} m^{-1} s^{-1}; d, 10^{-7} s^{-1} (dashed curve is 0.93×10^{-7} s^{-1}); $K_S{}^x$, 0.25×10^{-7} s^{-1}.

coefficients that result from linearization. Those of the crucial ocean thermal coefficients K_T and d, and the zonal wind stress coefficient K_S^x, are illustrated in Fig. 25; the strong zonal and meridional dependence contrasts markedly with the horizontally constant coefficients used in previous coupled ocean–atmosphere instability studies (e.g., Lau 1981; Philander et al. 1984; Hirst 1986, 1988). The effect of the strong zonal dependence of K_T is reflected in the disparate evolution of equatorial thermocline depth (h) and SST (T) anomalies shown in Figs. 6 and 7, where SST anomalies develop in situ while thermocline depth anomalies show a strong tendency for eastward propagation (cf. Hirst 1988, Figs. 10, 13). Such diverse patterns of h and T are possible because K_T is large in the east and very small in the west (Fig. 25). Windstress anomalies are restricted to the central basin, partly because of the position of the SST anomaly field, and partly because the zonal windstress coefficient K_S^x is largest in the central basin.

APPENDIX C

Evaluation of e^*

A precise evaluation of the coefficient e^* is difficult. Here, our main objective is to identify the effects of this principal nonlinearity, not justify a specific value. Thus, rather than obtaining a precise area averaged value for e^*, we wish to consider only the order of magnitude for e^*. We will evaluate e^* at 140°W on the equator, since it is only in the eastern Pacific where the full model h perturbations act nonlinearly in the T_s expression (4.2).

In the text, we have simplified the expression for T_s [cf., Eq. (4.2)],

$$T_s = \Theta(h)[\tanh(\lambda(\bar{h} + 1.5|h|)) - \tanh(\lambda\bar{h})] \quad \text{(C1)}$$

by approximating the asymmetric part of T_s with the cubic equation

$$T_s = a(\bar{h})h - e^*h^3 + O(h^5). \quad \text{(C2)}$$

With the cubic approximation to (C1), we would like to obtain roughly the same subsurface temperature perturbations Θ_c at the local extrema $h_c = (a/3e^*)^{1/2}$ of (C2) as that which is possible at infinite perturbation in (C1), given by

$$\Theta_{exe} = \Theta[1 - \tanh(\lambda\bar{h})].$$

Since Θ_{exe} is achieved at $|h| = \infty$ in (C2), h_c is arbitrarily defined as the displacement necessary to attain $0.9\Theta_{exe} \equiv \Theta_c$. As the value for Θ_c depends on the sign of the h perturbation, we equate h_c with the average value for $h_c = (h_c^+ - h_c^-)/2$, where the sign indicates the sense of the pycnocline perturbation. At 140°W, the parameter a, defined in B88, and has a value of 0.138°C m^{-1}, $\Theta_c = (\Theta_c^+ - \Theta_c^-)/2 = 3.3$°C and $h_c = 45$ m.

With a fixed in (C2), e^* is the only free parameter. Therefore, we are not able to fit both Θ_c and h_c. If we choose to calculate e^* by retaining h_c at 45 m, we estimate $e^* = ah_c^{-2}/3$ to be 2.27×10^{-5} °C m^{-2}. For this value of e^*, the maximum T_s obtained in (C2) at $h_c = 45$ is 4.1°C. This is comparable with the Θ_c. Alternatively, we can require that Θ_c be 3.3°C at $h = 45$ m, which yields $e^* = (a - \Theta_c/h)/h^2 = 3.19 \times 10^{-5}$ °C m^{-2}. Choosing this value for e^* sets h_c at 38 m. A compromise value for Θ_c is chosen at 3.7°C, and thus a value for e^* is obtained at 2.9×10^{-5} °C m^{-2} at $h_c = 40$ m.

REFERENCES

Battisti, D. S., 1988a: The dynamics and thermodynamics of a warm event in a coupled atmosphere/ocean model. *J. Atmos. Sci.*, **45**, 2889–2919.

——, 1988b: Interannual variability in the tropical atmosphere-ocean models. *Climate-Ocean Dynamics*, M. E. Schlesinger, Ed., Kluwer Press.

Bigg, G. R., and J. R. Blundell, 1988: The equatorial Pacific Ocean prior to and during El Niño of 1982/83—a normal mode model view. *Quart. J. Roy. Meteor. Soc.*, Submitted.

Cane, M. A., and R. J. Patton, 1984: A numerical model for low-frequency equatorial dynamics. *J. Phys. Oceanogr.*, **14**, 1853–1863.

——, and S. E. Zebiak, 1985: A theory for El Niño and the Southern Oscillation. *Science*, **228**, 1084–87.

Gill, A. E., 1980: Some simple solutions for heat-induced tropical circulation. *Quart. J. Roy. Meteor. Soc.*, **106**, 447–462.

Hirst, A. C., 1986: Unstable and damped equatorial modes in simple coupled ocean–atmosphere models. *J. Atmos. Sci.*, **43**, 606–630.

——, 1988: Slow instabilities in tropical ocean basin-global atmosphere models. *J. Atmos. Sci.*, **45**, 830–852.

Lau, K. M., 1981: Oscillations in a simple equatorial climate system. *J. Atmos. Sci.*, **38**, 248–261.

May, R. M., 1983: Nonlinear problems in ecology and resource management. Chaotic Behavior of Deterministic Systems, G. Iooss, R. H. G. Hellerman, R. Stora, Eds. North Holland.

McCreary, J. P., 1983: A model of tropical ocean–atmosphere interaction. *Mon. Wea. Rev.*, **111**, 370–387.

Philander, S. G. H., T. Yamagata and R. C., Pacanowski, 1984: Unstable air–sea interactions in the tropics. *J. Atmos. Sci.*, **41**, 604–613.

Saaty, T. L., 1981: Modern nonlinear equations. *Delay Differential Equations*, Dover, 213–261.

Schopf, P. S., 1987: Coupled dynamics of the tropical ocean-atmosphere system. *Further Progress in Equatorial Oceanography*, Nova Press, 279–286.

——, and M. J. Suarez, 1988: Vacillations in a coupled ocean–atmosphere model. *J. Atmos. Sci.*, **45**, 549–566.

Suarez, M. J., and P. S. Schopf, 1988: A delayed action oscillator for ENSO. *J. Atmos. Sci.*, **45**, 3283–3287.

Zebiak, S. E., 1986: Atmospheric convergence feedback in a simple model for El Niño. *J. Atmos. Sci.*, **114**, 1263–1271.

——, and M. A. Cane, 1987: A model El Niño/Southern Oscillation. *Mon. Wea. Rev.*, **115**, 2262–2278.